Analysis and comparison of three ecosystem models

P. A. Newberger, J. S. Allen, and Y. H. Spitz

College of Oceanic and Atmospheric Sciences, Oregon State University, Corvallis, Oregon, USA

Received 18 October 2001; revised 30 October 2002; accepted 5 November 2002; published 6 March 2003.

[1] Three-component (NPZ), four-component (NPZD), and five-component (NNPZD) nitrogen-based ecosystem models are compared. The fixed points of the zero-dimensional systems, with no spatial variation except light attenuation by water, are determined. A linear-stability analysis shows that unstable steady solutions exist for all three models. Time-periodic solutions are found in these regions. It is shown that the choice of the values of the parameters in the zooplankton equation is critical in determining steady state concentrations. One-dimensional model studies allowing variation with depth, self-shading by phytoplankton, and vertical diffusion show that the differences among the models increase when the available light is influenced by the presence of phytoplankton. With vertical diffusion, periodic solutions, such as those in the zero-dimensional case, are not found. Finally, a set of one-dimensional depth-integrated models, with variability in time and across-shore coordinate, are formulated. These models include horizontal advection and diffusion and the sinking of detritus (or phytoplankton). Application of a constant offshore advection velocity and coastal boundary conditions consistent with upwelling, produces many of the features seen in two-dimensional experiments [*Spitz et al.*, 2003]. The dependence of the resulting spatial distributions of phytoplankton and zooplankton on the values of the biological parameters is determined, helping to explain the two-dimensional results. Significant differences are found between the NPZ and the other models as a result of the sinking of phytoplankton rather than detritus. *INDEX TERMS:* 4815 Oceanography: Biological and Chemical: Ecosystems, structure and dynamics; 4842 Oceanography: Biological and Chemical: Modeling; 4279 Oceanography: General: Upwelling and convergences; *KEYWORDS:* coastal ecosystem modeling, numerical modeling, linear stability analysis

Citation: Newberger, P. A., J. S. Allen, and Y. H. Spitz, Analysis and comparison of three ecosystem models, *J. Geophys. Res.*, *108*(C3), 3061, doi:10.1029/2001JC001182, 2003.

1. Introduction

[2] Before using an ecosystem model coupled to a model of ocean physics, it is important to understand the underlying dynamics of the system of biological equations. We will look at various aspects of biological-physical model coupling with the goal of explaining the sources of differences among three simple ecosystem models. We will try to illustrate some of the ways that the forms of the equations and the choices of parameter values determine the behavior of the system. We examine the behavior of a three-component NPZ model (dissolved inorganic nitrogen *DIN*, phytoplankton *P* and zooplankton *Z*) [e.g., *Franks et al.*, 1986], four-component NPZD model (*DIN*, *P*, *Z* and detritus *D*) [e.g., *Denman and Peña*, 1999; *Edwards*, 2001] and five-component NNPZD model (nitrate NO_3, ammonium NH_4, *P*, *Z*, *D*) [e.g., *Wroblewski*, 1977]. These models are coupled with the primitive-equation Princeton ocean model (POM) in a companion paper [*Spitz et al.*, 2003]. The coupled model is used to simulate the ecosystem in the Oregon coastal upwelling zone in a two-dimensional (variation across-shore x and with depth z, uniformity alongshore) approximation. We will show how study of the solution properties of the ecosystem-model equations in idealized situations can provide helpful insight into the interpretation of realistic simulations. For consistency, the models have been modified to use the same parameterization of each of the ecosystem interactions so that the differences among the models arise primarily from the constituents included.

[3] In section 2 of this paper we will look at the equations at a single point in space, that is, with only the light varying with water depth. In section 3 we will look at the fixed points of each of the three ecosystem models and calculate the linear stability about the fixed points. The differences in behavior of the models and the dependence of these results on some of the parameters will be described in section 4. We will then examine the depth-varying behavior of these models (one space dimension, variation with depth z) in section 5. *Edwards et al.* [2000] have examined the dynam-

0148-0227/03/2001JC001182$09.00

Table 1. Parameters Used in This Study[a]

Symbol	Description	Values	Units
k_w	light attenuation by sea water	0.067	m^{-1}
k_P	light attenuation by phytoplankton	9.5 10^{-3} (0)	$m^2(mmol\ N)^{-1}$
α	initial slope of the $P-I$ curve	0.025	$(W\ m^{-2}\ d)^{-1}$
V_m	phytoplankton maximum uptake rate	1.5	d^{-1}
I_0	surface photosynthetically available radiation	158.075	$W\ m^{-2}$
K_u	half-saturation for phytoplankton uptake of nutrients	1.0	$mmol\ N\ m^{-3}$
Ψ	NH_4 inhibition parameter	1.46 (0)	$(mmol\ N\ m^{-3})^{-1}$
Ξ	phytoplankton specific mortality rate	0.1	d^{-1}
R_m	zooplankton maximum grazing rate	0.52 (1.5)	d^{-1}
Λ	Ivlev constant	0.06	$(mmol\ N\ m^{-3})^{-1}$
γ	fraction of zooplankton grazing egested	0.3	
Γ	zooplankton specific excretion/mortality rate	0.145	d^{-1}
Φ	detritus decomposition rate	1.03 (0.175)	d^{-1}
Ω	NH_4 oxidation rate	0.25 (0.041)	d^{-1}
w_d	sinking rate for detritus	0.0 (8.0, 1.0)	$m\ d^{-1}$
w_p	sinking rate for phytoplankton	0.0 (0.65)	$m\ d^{-1}$

[a]The first value listed for each parameter is that used in the basic-case study. Other values used are enclosed in parentheses. The parameters Ψ and Ω are only used in the NNPZD model; Φ does not occur in NPZ. The detritus sinks with velocity w_d in NPZD and NNPZD, while phytoplankton sinks with velocity w_p in NPZ.

ics of an NPZ model in a one-dimensional setting with and without vertical diffusion. We will look at the behavior of the additional models in this context. The effect of the decreased light caused by self-shading by the phytoplankton will be included. Finally, in section 6, we will employ a simple depth-averaged, biological-physical, surface layer model (one space dimension, variation across-shelf x) to explain features and differences seen in the two-dimensional POM-ecosystem coupled model results of *Spitz et al.* [2003]. In particular, this surface layer model includes the effects of advection and of sinking one component (phytoplankton for the NPZ model, detritus for NPZD and NNPZD) and illustrates important differences in the model solutions that are not found in the case of zero dimensions or of variations only with depth. Section 7 includes a summary and discussion of results.

2. Ecosystem Equations

[4] The NNPZD system considered in this study is based on that of *Wroblewski* [1977] and is given by

$$\frac{dP}{dt} = G\left(\frac{NO_3}{K_u + NO_3}e^{-\Psi NH_4} + \frac{NH_4}{K_u + NH_4}\right)P - R_m\left(1 - e^{-\Lambda P}\right)Z - \Xi P, \quad (1)$$

$$\frac{dZ}{dt} = (1-\gamma)R_m\left(1 - e^{-\Lambda P}\right)Z - \Gamma Z, \quad (2)$$

$$\frac{dD}{dt} = \gamma R_m\left(1 - e^{-\Lambda P}\right)Z + \Xi P - \Phi D, \quad (3)$$

$$\frac{dNH_4}{dt} = \Phi D + \Gamma Z - G\frac{NH_4}{K_u + NH_4}P - \Omega NH_4, \quad (4)$$

$$\frac{dNO_3}{dt} = \Omega NH_4 - G\frac{NO_3}{K_u + NO_3}e^{-\Psi NH_4}P, \quad (5)$$

where the parameter definitions and the parameter values are given in Table 1. The value of each parameter is chosen to be appropriate to the oceanographic ecosystem in the upwelling region off the coast of Oregon [*Wroblewski*, 1977; *Spitz et al.*, 2003]. In addition we define

$$G = V_m \times f(z,t), \quad (6)$$

$$f(z,t) = \frac{\alpha I}{\left(V_m^2 + \alpha^2 I^2\right)^{\frac{1}{2}}}, \quad (7)$$

$$I(z) = I_0\ \exp\left[k_w z + k_P \int_0^z P(z')dz'\right], \quad (8)$$

where $-H < z < 0$ is the water depth. Adding equations (1)–(5) shows that the total,

$$T_5 = P + Z + NO_3 + NH_4 + D, \quad (9)$$

is constant.

[5] In the NPZD system that is based on that of *Denman and Peña* [1999], equation (1) is replaced by

$$\frac{dP}{dt} = G\frac{DIN}{K_u + DIN}P - R_m\left(1 - e^{-\Lambda P}\right)Z - \Xi P, \quad (10)$$

and equations (4) and (5) are replaced by

$$\frac{dDIN}{dt} = \Phi D + \Gamma Z - G\frac{DIN}{K_u + DIN}P, \quad (11)$$

so that the governing equations are (2), (3), (10) and (11) with the constant total

$$T_4 = P + Z + DIN + D. \quad (12)$$

[6] In the NPZ system [*Franks et al.*, 1986], equation (11) is replaced by

$$\frac{dDIN}{dt} = \Xi P + \Gamma Z - G\frac{DIN}{K_u + DIN}P + \gamma R_m\left(1 - e^{-\Lambda P}\right)Z, \quad (13)$$

so that the governing equations are (2), (10) and (13) with constant total

$$T_3 = P + Z + DIN. \tag{14}$$

3. Fixed Points and Linear Stability

[7] The dynamics of the NPZ model are described in detail by *Busenberg et al.* [1990] They determine the fixed points (steady solutions, all time derivatives identically zero) of the system and the linear stability of each as a function of the parameters and in most cases the range of attraction and nature of the long time behavior. In this work we are primarily interested in the differences among the three models and in understanding how these differences influence the results of coupled physical circulation and ecosystem models. A complete and rigorous treatment of the dynamics of the four- (NPZD) and five- (NNPZD) equation models is beyond the scope of this paper. We will examine here the fixed points and linear stability of the models numerically at the basic-case parameter values of Table 1. The analysis for some additional parameter values is included in Appendix A. In this section the phytoplankton self-shading will be neglected so that in equation (8), $k_P = 0$. The description of the NPZ model by *Busenberg et al.* [1990] will be used as a guide and as a comparison.

3.1. Fixed Points

[8] The number of fixed points of systems of equations such as the NNPZD is not known in advance and depends in fact on the choice of parameter values. A graphical method of determining the approximate location of the fixed points has been developed and used in this study. This graphical method is used to provide a starting point for a Newton's method [e.g., *Press et al.*, 1992] determination of the fixed points. The equations are then linearized about the fixed points and the linear stability is determined. These equations have fixed points where the concentration of one or more of the constituents is negative, which is not biologically sensible. Only biologically sensible fixed points with all constituents ≥ 0 will be considered in this analysis.

[9] The fixed points of the NPZ and NPZD system are determined analytically. For NPZ the fixed points are given by the solutions of the following two equations in P and DIN that are equations (10) and (2) with time derivatives set to zero:

$$0 = G\frac{DIN}{K_u + DIN}P - R_m\left(1 - e^{-\Lambda P}\right)Z - \Xi P, \tag{15}$$

$$0 = (1-\gamma)R_m\left(1 - e^{-\Lambda P}\right)Z - \Gamma Z, \tag{16}$$

where $Z = T_3 - P - DIN$, with T_3 the specified total nitrogen (mmol N m^{-3}). G is defined in equation (6) and the parameters are given in Table 1. Examination of equation (16) shows that there are two types of solutions to these equations: those with $Z = 0$, and those with $Z \neq 0$ and P satisfying equation (16). In the first case, $Z = 0$ and either $P = 0$ or, from equation (15) with $Z = 0$ and $P = T_3 - DIN$,

$$DIN = \frac{K_u \Xi}{G - \Xi}. \tag{17}$$

This solution is biologically sensible whenever $G > \Xi$ and $T_3 > DIN$.

[10] The only solutions with $Z \neq 0$ have constant phytoplankton $P = P^*$ where, from equation (16),

$$P^* = -\frac{1}{\Lambda}\ln\left[1 - \frac{\Gamma}{(1-\gamma)R_m}\right]. \tag{18}$$

The non-zero values of $Z = Z^*$ at $P = P^*$ are the positive, biologically feasible roots of the quadratic equation obtained from equation (15) by using equation (14) to eliminate DIN,

$$R_m\left(1 - e^{-\Lambda P^*}\right)Z^{*2} - Z^*\left[R_m\left(1 - e^{-\Lambda P^*}\right).\left(K_u + T_3 - P^*\right) - (\Xi - G)P^*\right] + P^*\left[(G - \Xi)\left(T_3 - P^*\right) - K_u\Xi\right] = 0. \tag{19}$$

Busenberg et al. [1990] show that there will be at least one positive root if $G - \Xi > 0$ and $T_3 - P^* > 0$. They show that both roots are positive if $(G - \Xi)(T_3 - P^*) > K_u\Xi$ and that exactly one root corresponds to a solution with all the constituents having nonnegative values.

[11] For the NPZD, equations (15) and (16) still follow from equations (10) and (2) and solutions are determined analytically. The fixed point values of D can be written as functions of P and Z from equation (3) as

$$D = \frac{\gamma R_m\left(1 - e^{-\Lambda P}\right)Z + \Xi P}{\Phi}. \tag{20}$$

The fixed point values of Z are written as a function of T_4, DIN and P from equation (12) eliminating D with equation (20),

$$Z = \frac{T_4 - DIN - \left(1 + \frac{\Xi}{\Phi}\right)P}{1 + \frac{\gamma}{\Phi}R_m\left(1 - e^{-\Lambda P}\right)}. \tag{21}$$

If $Z = 0$, $P + D = T_4 - DIN$, DIN satisfies equation (17) and from equation (3),

$$D = \frac{\Xi}{\Phi}P, \tag{22}$$

except in the case that $P = D = Z = 0$. Again, if $Z \neq 0$, $P = P^*$ where P^* satisfies equation (18) and $Z^* \neq 0$ is given by the positive roots of the quadratic equation, obtained from equation (15) by using equations (12) and (20) to eliminate DIN and D,

$$C_2R_m\left(1 - e^{-\Lambda P^*}\right)Z^{*2} - Z^*\left[R_m\left(1 - e^{-\Lambda P^*}\right) \cdot \left(K_u + T_4 - C_1P^*\right)C_2(\Xi - G)P^*\right] + P^*\left[(G - \Xi) \cdot \left(T_4 - C_1P^*\right) - K_u\Xi\right] = 0, \tag{23}$$

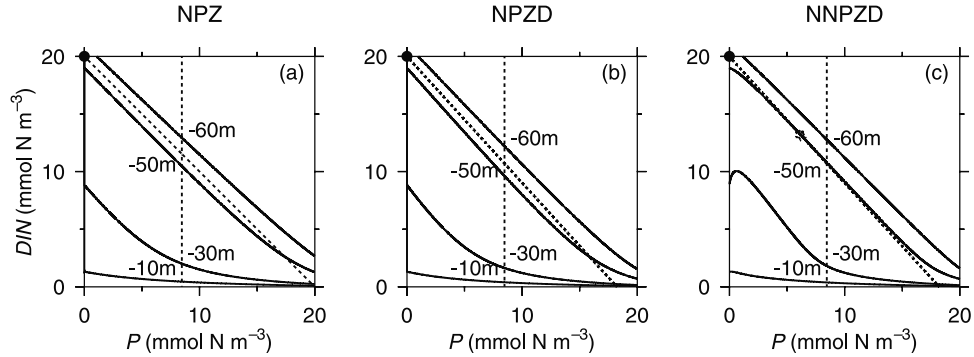

Figure 1. Plots to find the approximate locations of the fixed points for (a) NPZ system, (b) NPZD system, and (c) NNPZD system with the basic-case parameter values. Solutions are shown for $T = 20$ mmol N m^{-3} and at depths $z = -10$, -30, -50 and -60 m. The dashed lines are the zeros of equation (16) with the vertical line corresponding to $P = P^*$ and the diagonal to $Z = 0$. The solid curves are solutions to equation (15) (NPZ and NPZD) or (25) (NNPZD) at the different depths. The solutions with $DIN = T$, $P = 0$ are marked with a bullet. The other fixed points are located at the intersections of the solid and dashed lines. For clarity the solution for the NNPZD at $z = -50$ m is marked with a star.

where

$$C_1 = 1 + \frac{\Xi}{\Phi} \quad \text{and}$$
$$C_2 = 1 + \frac{\gamma}{\Phi} R_m \left(1 - \mathrm{e}^{-\Lambda P^*}\right) = 1 + \frac{\gamma\Gamma}{\Phi(1-\gamma)}. \tag{24}$$

The arguments of *Busenberg et al.* [1990] can be extended to show that there is at least one positive root if $G - \Xi > 0$ and $T_4 - C_1P^* > 0$. From equation (20) we see that C_1P^* is the sum of P^* and the part of the detritus D coming from the phytoplankton so that $T_4 > C_1P^*$ for all biologically feasible solutions. Both solutions are positive if $(G - \Xi)(T_4 - C_1P^*) > K_u\Xi$. The method of *Busenberg et al.* [1990] applied to this system of equations shows that exactly one of these solutions is biologically feasible.

[12] In the NNPZD system, equation (10) is replaced by equation (1) and thus equation (15) is replaced by

$$0 = G\left(\frac{NO_3 \mathrm{e}^{-\Psi NH_4}}{K_u + NO_3} + \frac{NH_4}{K_u + NH_4}\right) P - R_m\left(1 - \mathrm{e}^{-\Lambda P}\right) Z - \Xi P, \tag{25}$$

which follows from equation (1) with zero time derivative. Z satisfies equation (21) with $DIN = NO_3 + NH_4$, D satisfies equation (20) with T_5 replacing T_4, and from equation (5),

$$NO_3 = \frac{-K_u \Omega NH_4}{\Omega NH_4 - GP\mathrm{e}^{-\Psi NH_4}}, \tag{26}$$

unless $NH_4 = 0$ in which case $P = Z = D = 0$ and $NO_3 = T_5$.

[13] Newton's method [e.g., *Press et al.*, 1992] is used to find the steady solutions numerically for the NNPZD system of equations. A graphical method to find the approximate location of the fixed points consists of calculating and contouring the values of the right hand sides of equations (16) and (25) as functions of DIN and P in the range $0 < DIN < T_5$ and $0 < P < T_5$. For each of the equations, the zero contour is the solution and the intersections of the zero contours of the two equations are the solutions of the system. Given P, DIN and T_5, we calculate Z from equation (21), NO_3 iteratively from equation (26) and $NH_4 = DIN - NO_3$. The right-hand sides of equations (16) and (25) are evaluated at these values and the results are contoured to obtain the approximate solutions. The approximate solutions are then used as initial values in an accurate, Newton's method calculation of the fixed points. Although the solutions for NPZ and NPZD can be calculated directly, this method will be used with the simpler models as well so that the fixed-point behavior of each of the three models can be compared easily.

[14] Note that equation (16) is the same for the three models and has no dependence on G and thus no depth dependence. The only solutions are $P = P^*$, a vertical line in the (P, DIN) plane, or $Z = 0$. For the NPZ model, the $Z = 0$ solution is the line in the (P, DIN) plane given by $P + DIN = T_3$. For NPZD and NNPZD, $Z = 0$ is the line $P(1 + \frac{\Xi}{\Phi}) + DIN = T_{4,5}$ from equation (20) and either equation (12) for the NPZD or equation (9) for NNPZD. The fixed points are given by the intersections of either of the $P = P^*$ line or the $Z = 0$ line with the zero contours of equation (25) for NNPZD or of equation (15) for NPZ and NPZD. The region of the (P, DIN) plane with $P > 0$, $DIN > 0$ and below the $Z = 0$ line contains all of the biologically feasible solutions. Note that there are no feasible $Z \neq 0$ solutions unless $T > P^*$ for the NPZ or $T > C_1P^*$ for the NPZD or NNPZD.

[15] Figure 1 shows the location of the fixed points of the three models at four depths for $T_{3,4,5} = 20$ mmol N m^{-3}. This value is chosen to be within the range of concentrations found near the Oregon coast during upwelling [*Spitz et al.*, 2003]. The dashed lines are the solutions to equation (16) and are independent of depth. The solid curves are the solutions to equation (25) or equation (15) at each of the four depths. The dependence on depth enters through the variation of light with depth in equation (8). The $DIN = T$ solution marked by a bullet in the upper left-hand corner is a fixed point at all depths. For the basic-case parameter values, $P^* \approx 8.468$ and depends only on the

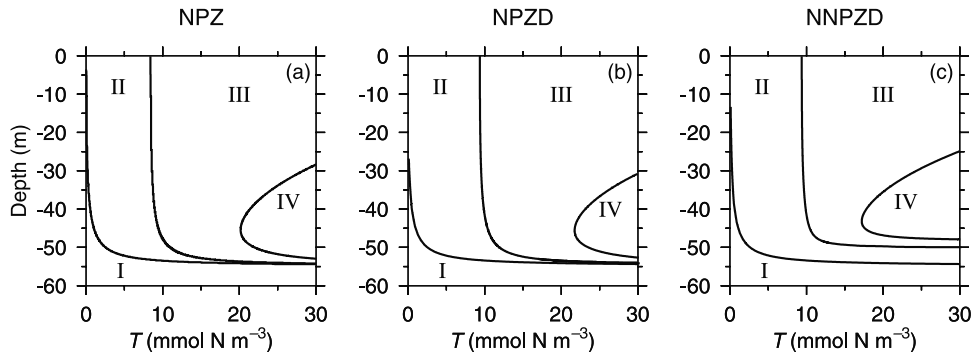

Figure 2. (a) Regions of stability as explained in the text of the fixed points for NPZ. (b) Numerical calculation of regions of stability of the fixed point of NPZD, and (c) the same for NNPZD.

value of the parameters Λ, Γ, γ and R_m that occur in equation (18). These figures show that each of these models has three fixed points at each of the depths shown. There is the $DIN = T$ solution, one $P = P^*$, $Z \neq 0$ solution and one $P \neq 0$, $Z = 0$ solution for each model at each depth. The locations of the fixed points vary among the models, but the general pattern of the solutions is similar in all cases. The intersection of the $P = P^*$ line and the solution to equation (25) or equation (15) for depths greater than a critical depth (about -52.4 m for NPZ and NPZD and -50 m for NNPZD) are fixed points, as shown for $z = -60$ m. These points lie above the dashed $Z = 0$ diagonal line so that the concentration of zooplankton at these depths is negative. These biologically meaningless solutions are not considered further.

3.2. Linear Stability of Fixed Points

[16] With the number and approximate location of the fixed points determined graphically, Newton's method is used to find the values of the fixed points. A fixed-point is stable if an integration of the equations forward in time starting at every initial condition sufficiently near the fixed point converges to the fixed-point values. If the fixed point is unstable, the solution may tend to a different, stable, fixed point or it may oscillate periodically or in some cases aperiodically around an unstable fixed point. A linear-stability analysis determines what behaviors will occur for small perturbations of the fixed-point solution.

[17] The eigenvalues of the stability matrix at each fixed point are calculated to determine the linear stability [*Nayfeh and Mook*, 1979]. As noted above, the fixed points of the NPZ and NPZD are given by algebraic equations. *Busenberg et al.* [1990] explicitly calculate the stability matrix and eigenvalues for each of the fixed points of NPZ and determine the stability as a function of the parameters. Figure 2a shows their stability results in the special case of the basic-case parameter values given in Table 1 and with the dependence of phytoplankton growth rate on depth used in this study. The depth z enters only through the variation of light with depth so that the details of these results will depend on the form chosen for this dependence (equation (8)). Figures 2b and 2c show the same results for the NPZD and NNPZD models. These were determined numerically using Newton's method to find the fixed points as a function of depth (z) and total nitrogen (T) and then calculating the stability of each fixed point.

[18] Region I of Figure 2a is the region where the $DIN = T$ fixed point is stable. This solution always exists but is stable for the NPZ only for very small T or regions of depth with insufficient light to support phytoplankton. Numerical results displayed in Figures 2b and 2c show a similar region of stability for NPZD and NNPZD for this solution. For z and T in this range, integration of the equations with any initial conditions consistent with T will converge to this solution. Any phytoplankton and zooplankton will die, detritus will decompose and ammonium will be oxidized.

[19] Region II of Figure 2a is the region of stability of the $Z = 0$, $P \neq 0$ solution for NPZ where DIN takes a value such that the phytoplankton growth is equal to the mortality (equation (17)). This solution is found to be stable when it exists if the fixed-point value of the phytoplankton $P < P^*$ [*Busenberg et al.*, 1990]. For the NPZ this is equivalent to P^* being biologically unfeasible. Numerical calculations of eigenvalues and stability for NPZD and NNPZD find that the same conditions imply stability for the $Z = 0$, $P \neq 0$ solution for this set of parameter values. For example, the fixed points with large phytoplankton concentrations at $z = -10$ m and -30 m shown in Figures 1a, 1b, and 1c have $P > P^* = 8.468$, $Z = 0$ and are found to be unstable. In contrast, there is a stable fixed point, marked by a star in Figure 1c, of NNPZD at $z = -50$ m with $P = 6.18$ mmol N m^{-3} and with P^* outside the region of feasibility. Integration of the zero-dimensional ecosystem equations for T and z in region II that have non-zero phytoplankton initially will converge to solutions with $0 < P < P^*$ and $Z = 0$.

[20] In regions III and IV the $P = P^*$, $Z \neq 0$ solution exists and is feasible. This solution is found to be stable in region III and unstable in region IV. For example at $T = 20$ mmol N m^{-3} all biologically feasible fixed points of this type are stable for the NPZ and NPZD models (Figures 2a and 2b). In the case of the NNPZD the line $T = 20$ mmol N m^{-3} intersects region IV of Figure 2c showing that there are unstable fixed points at some intermediate depths. In region IV, the eigenvalues with positive real part indicating instability are complex conjugate pairs, which suggests oscillatory behavior (see Appendix B for a discussion of oscillating solutions for the NPZ). Integration of the zero dimensional ecosystem equations shows that the long time solutions in this range of z and T are limit cycles. The period of these cycles determined by this integration of the zero-

dimensional equations increases with depth. For NNPZD and $T = 20$ mmol N m^{-3} the period increases from about 48 days at 35.5 m to about 120 days at 46.5 m. Similar patterns are seen for the other two models. In all cases tested, the imaginary part of the eigenvalue is an accurate predictor of the period of the limit cycle.

3.3. Model Comparison

[21] The biggest differences among the models shown in Figures 1 and 2 are that the P^* solution reaches the limit of feasibility at a shallower depth for the NNPZD (region III is less deep) and unstable fixed points (region IV) are found at smaller values of T. It is also found that the amount of zooplankton supported at a given depth is greatest for the NPZ and least for the NNPZD. For example, for $T = 20$ mmol N m^{-3} for the three models $Z = 11.1$, 9.7 and 9.3 mmol N m^{-3} at $z = -10$ m, $Z = 9.5$, 8.6 and 8.4 mmol N m^{-3} at -30 m and $Z = 1.1$, 1.0 and 0 mmol N m^{-3} at -50 m, respectively.

[22] For the NPZ and NPZD, equation (17) shows that there is only one solution with $Z = 0$ and $P \neq 0$ at each depth. Figure 1c indicates that this is true for the NNPZD as well except possibly when the $Z = 0$ line and the equation (25) curve are nearly tangent as shown near $z = -50$ m. The location of the solution found at that depth is marked with a star. Numerical experiments for NNPZD have not found a second solution with $Z = 0$ and $P \neq 0$ for the basic-case choice of parameter values. As shown in Appendix A, this result in not true in general for the NNPZD.

[23] Numerical examination of the properties of fixed points of three ecosystem models has illustrated some differences in the models. With the basic-case parameter values, however, the similarities are much greater than the differences among the three models. In fact, the NPZ and NPZD models are found to behave nearly identically with a slightly larger zooplankton concentration found in the NPZ. This is consistent with the results of *Edwards* [2001], who finds that the effect of adding detritus to a differently formulated NPZ model is small if there is no zooplankton grazing on the detritus as is the case in our formulation. With no inhibition in NO_3 uptake ($\Psi = 0$ (mmol N m^{-3})$^{-1}$) in the presence of NH_4, the NNPZD solutions (Appendix A) are significantly different from those of the other models and from the NNPZD basic-case solution especially near the bottom of the biologically active zone. This change of a single parameter in the NNPZD model makes more difference in the zero dimensional steady solutions than is found among the three models with the basic-case parameter values.

4. Sensitivity to Choice of Parameter Values

[24] To better understand the sensitivity of the models to the choice of parameter values, we examine the $P = P^* \neq 0$, $Z \neq 0$ steady solutions as a function of each of the parameters separately. In each case, we vary the parameter about the basic-case values of Table 1. This provides a first look at the parameter dependence in the range of interest for modeling the Oregon coastal environment. The terms of the equations interact, however, so that this technique will not give the whole story. It is useful to determine which of the parameters have a strong effect on the nature of the steady solution and which have little effect over a wide range of values. As noted above, the value of $P = P^*$ will change only if the parameters in equation (2), that is, γ, R_m, Λ and Γ are varied. The fixed-point values of the other components may change with each parameter.

[25] The variation of the fixed-point solutions for each of the parameters has been calculated for all three models at three values of T (30, 20 and 10 mmol N m^{-3}) at $z = -10$ m. In addition the same calculations have been made for $z = -40$ m for the NNPZD. All of the solutions considered have $P \neq 0$ and are biologically feasible. These depths are selected to illustrate the behavior in two depth ranges. In the top 15 to 20 m the concentrations vary slightly with depth. Deeper, near $z = -40$ m, the phytoplankton concentration remains constant at $P = P^*$, but a reduced amount of zooplankton can be supported and the concentrations of the other constituents vary significantly with depth.

[26] Figure 3 shows those parameters that have been found to most significantly influence the concentrations at the fixed point at a depth of -10 m. The basic-case value of each parameter is marked by a horizontal white line. The results for the three models are shown for $T = 20$ mmol N m^{-3}. The differences in sensitivity to the parameter changes are small for the three models at $T_{3,4,5} = 20$ mmol N m^{-3}. This is typical of the results for the other concentrations that are not shown for NPZ or NPZD.

[27] Increasing the mortality rate for zooplankton Γ (d^{-1}) or the fraction of grazing that is egested γ, results in a decrease in zooplankton concentration and increase in phytoplankton as expected intuitively. The dependences on the maximum grazing rate R_m (d^{-1}) and the Ivlev constant Λ [(mmol N m^{-3})$^{-1}$] are more complicated. A maximum zooplankton concentration may be present for intermediate values of these parameters. For the Ivlev constant Λ, this occurs for the largest total T. In the other cases, the zooplankton concentration increases and the phytoplankton concentration decreases as Λ increases. For the grazing rate R_m, a maximum in zooplankton concentration is found at intermediate values for both $T = 20$ and $T = 30$ mmol N m^{-1}. In particular, we note that at the basic-case value $R_m = 0.52$ d^{-1} used in this study the zooplankton concentration is near the maximum for $T = 30$ mmol N m^{-3}. For $T = 10$ mmol N m^{-3} the zooplankton concentration is small for this value of R_m.

[28] At $R_m = 1.5$ d^{-1} (Appendix A) where P^* is small, the zooplankton concentration is only slightly reduced between $T = 30$ and $T = 10$ mmol N m^{-3}. We consider these two values of R_m as representative of a change in the zooplankton community from macrozooplankton for $R_m = 0.52$ d^{-1} to microzooplankton for $R_m = 1.5$ d^{-1} [*Spitz et al.*, 2003]. For the basic-case parameters values used in this study, $P^* = 8.468$ mmol N m^{-3} is large so T must be moderately large ($T > P^*$) to support any zooplankton. At $T = 10$ mmol N m^{-3}, small changes in the value of any of the parameters may result in no zooplankton in the steady state solution as shown for the NNPZD in Figure 3.

[29] Figure 4 shows the dependence of the fixed-point concentrations for the NNPZD at $z = -40$ m on the values of 10 parameters (Table 1). The basic-case value of each parameter is marked by a horizontal white line. The dependence on the value of the parameters Γ, R_m, γ and Λ that occur in the zooplankton equation are shown in the top four

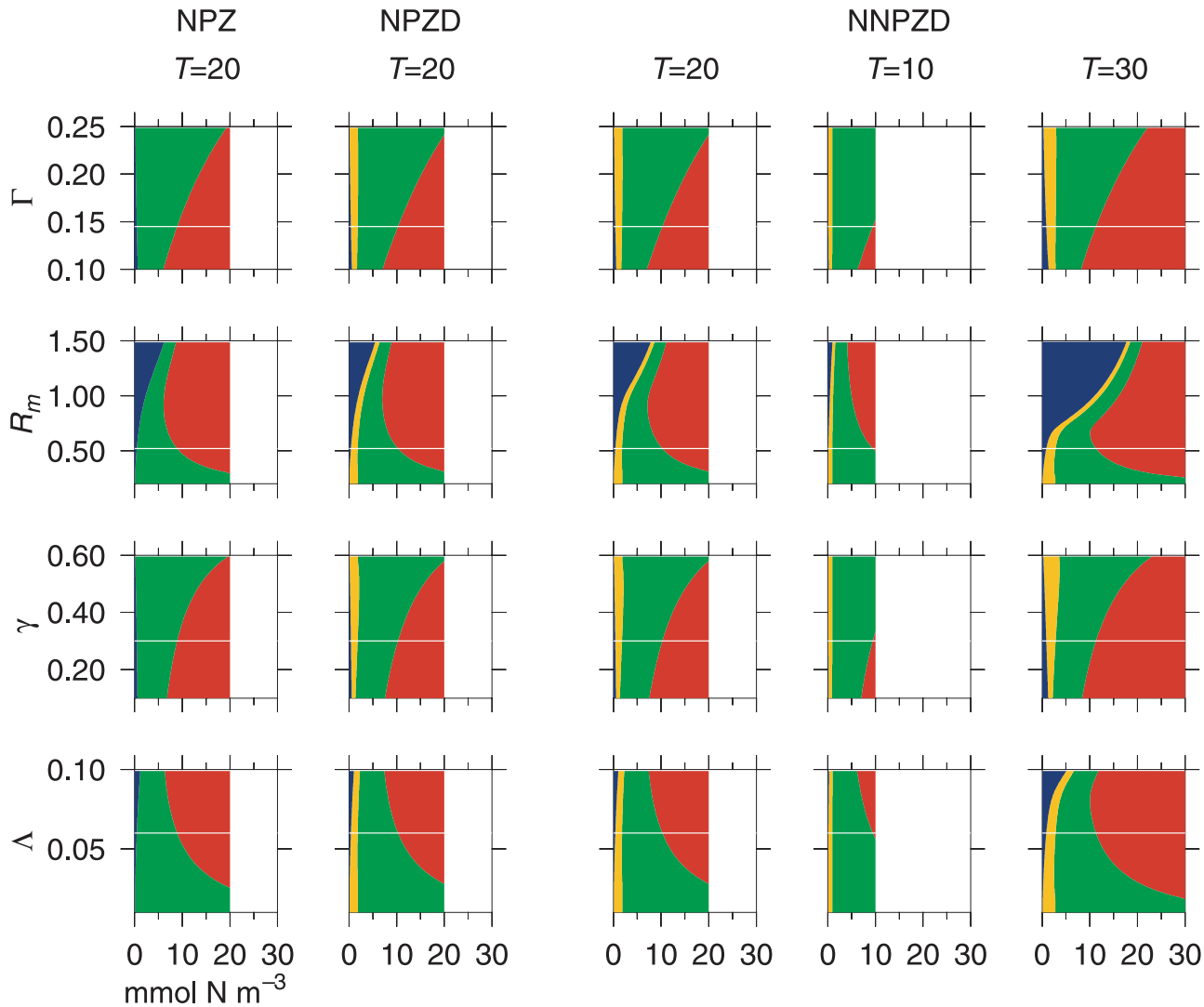

Figure 3. Amount of each constituent at the feasible $P \neq 0$ fixed point as a function of parameter value at a depth of $z = -10$ m. The blue region is the total *DIN*. Green is phytoplankton, red is zooplankton and yellow is detritus. Concentrations for all three models are shown for $T = 20$ mmol N m^{-3}. Only the results for the NNPZD are shown for $T = 10$ and $T = 30$ mmol N m^{-3}. The basic-case parameter value is marked with a horizontal white line (see Table 1 for definitions and units of the parameters).

of the left-hand panels. The dependences on the values of K_u, α, Ψ and Ξ that occur in the phytoplankton equation and have an appreciable effect on the concentrations at this depth are shown in the top four right-hand panels. In addition, the dependences on the parameter values of Φ and Ω, that together with Ψ define the differences among the models, are shown in the bottom row. The calculations are made for the NNPZD model as it is the one that involves all of the parameters. The qualitative behavior of the three models is sufficiently similar that this figure is indicative of the sensitivity to parameter variations of the each of the models for the relevant parameters.

[30] All of the parameters that cause large changes in the fixed points at $z = -10$ m (Figure 3) are also important at $z = -40$ m (Figure 4, the top four left-hand panels showing the dependence on the values of Γ, R_m, γ and Λ). At this depth the nutrients are not, in general, depleted and most of the change in phytoplankton concentration is reflected in changes in the nutrient concentration. The zooplankton concentration is smaller and less sensitive to changes in the parameters than it is at $z = -10$ m. In the $T = 10$ mmol N m^{-3} case, not shown, zooplankton concentrations are zero over much of the parameter range for each of the parameters.

[31] The additional parameters Ψ [(mmol N m^{-3})$^{-1}$], α [(W m^2 d)$^{-1}$], K_u (mmol N m^{-3}) and Ξ (d^{-1}), from the phytoplankton equation cause significant variations at $z = -40$ m (Figure 4). The phytoplankton concentration is constant as these parameters are varied as long as the zooplankton concentration remains non-zero. The concentration of zooplankton increases if the effect of the parameter change is to increase the difference between the growth term and the mortality term in the phytoplankton equation (which occurs as K_u decreases, α increases, Ψ decreases and Ξ decreases) where K_u, α and Ψ govern the uptake of nutrients by phytoplankton and Ξ is the phytoplankton

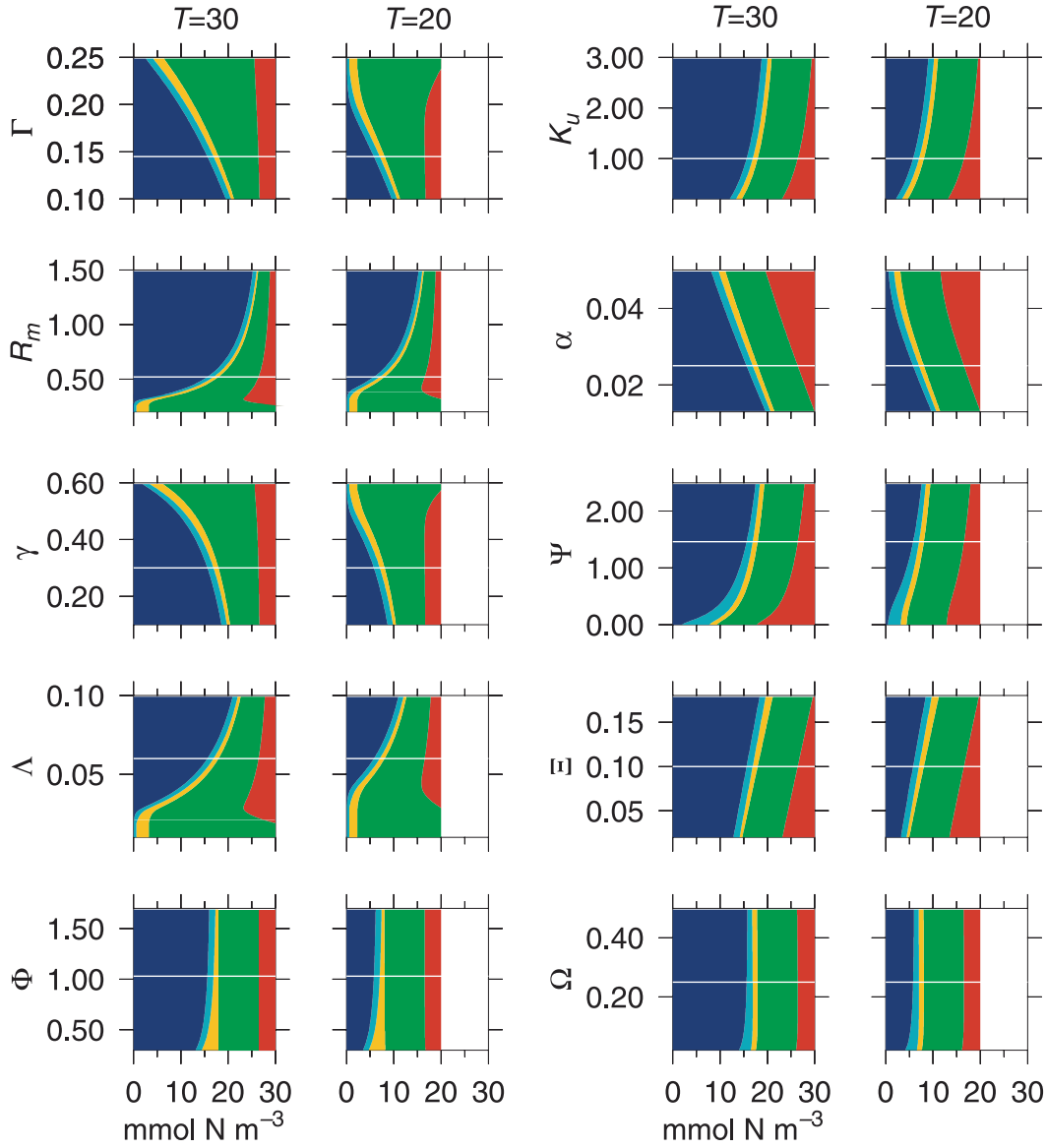

Figure 4. Amount of each constituent at the feasible $P \neq 0$ fixed point as a function of parameter values at a depth of $z = -40$ m for NNPZD. The colors are as in Figure 3 except that *DIN* is divided into NO_3 (blue) and NH_4 (light blue). The basic-case parameter value is marked with a horizontal white line (see Table 1 for definitions and units of the parameters).

mortality rate. Note that α only occurs multiplied by the light parameter, $I(z)$ (equation (7)) so that the dependence on α can be interpreted as the dependence on available light.

[32] The parameters Φ (d^{-1}), the detritus decomposition rate, and Ω (d^{-1}), the NH_4 oxidation rate that, together with Ψ, define the differences among the models are also of interest (Figure 4, bottom row). Near the basic-case parameter values, varying either Φ or Ω does not cause significant changes in the fixed-point solutions. The rate of detritus decomposition Φ represents the difference between the NPZ and NPZD models. It determines how quickly the detritus becomes available to the phytoplankton as nutrient. The NPZ solutions are the limit of the NPZD solutions for very large values of Φ, that is, instantaneous remineralization. This parameter has a small influence on the amount of zooplankton at $z = -10$ m with a slight decrease in zooplankton and nutrients and an increase in detritus for small values of Φ. At $z = -40$ m the increase in detritus as Φ decreases is balanced by the decrease in nutrients and zooplankton is essentially unchanged.

[33] The two parameters Ψ, discussed above and in Appendix A, and the NH_4 oxidation rate Ω (d^{-1}), which are found only in the NNPZD model, determine the interaction between the two nutrients in that model. For large values of Ω, essentially all of the nutrient is NO_3 and the NNPZD and NPZD agree closely for all values of Ψ. The choice of this parameter over a range of values around $\Omega = 0.25$ d^{-1} with the other parameters at their basic-case values determines the relative amount of NH_4 and NO_3 making up the *DIN*. This effect is small and there is insignificant change in the total *DIN* or in the other constituents when

$Z \neq 0$. At depths greater than 50 m where $P \neq 0$ but $Z = 0$, P decreases as Ω decreases (Appendix A).

5. Variation in the Vertical

[34] To this point, we have ignored any spatial variation except the attenuation of light by water. In this section we will consider the ecosystem models as a function of time and the vertical space dimension z (1D models). This will allow the inclusion of the light attenuation by self-shading by the phytoplankton and the inclusion of vertical diffusion. This one-dimensional study provides one bridge between the zero dimensional case with only light dependence and the two dimensional (x, z) study of *Spitz et al.* [2003] that includes realistic physics.

[35] The initial condition for these studies have $T(z, t = 0) = T_0(z)$ = 10 mmol N m^{-3} at the surface increasing linearly to 30 mmol N m^{-3} at 100 m and then to 35 mmol N m^{-3} at 500 m mimicking a non-upwelling situation on the Oregon shelf. The total nitrogen $T_0(z)$ is the sum of the constituents for each of the models. A 1D model without vertical diffusion or phytoplankton self-shading is essentially a stack of zero dimensional models with no interaction between different depths. With phytoplankton self-shading the concentrations above influence those below, but with no vertical diffusion the total nitrogen remains constant in time at each depth. The inclusion of vertical diffusion adds a term to each of the equations of the form

$$\frac{\partial B}{\partial t} = \text{Biology terms} + \frac{\partial}{\partial z} K_B \frac{\partial B}{\partial z}, \tag{27}$$

where B is any of the constituents of the ecosystem model. We will take the vertical diffusion coefficient K_B to be a constant. Steady states of the 1D biological equations with vertical diffusion have the same total concentration of nitrogen at each depth since addition of the ecosystem equations including vertical diffusion leads to

$$\frac{\partial T}{\partial t} = \frac{\partial}{\partial z} K_B \frac{\partial T}{\partial z}, \tag{28}$$

with boundary conditions

$$K_B \frac{\partial T}{\partial z} = 0, \tag{29}$$

at the surface and at the bottom, which for $\partial T/\partial t = 0$, implies that T is constant with depth. In this study we will take K_B small so that the timescale of the vertical diffusion is long compared to the timescale of the biological adjustment. We look at solutions with the biological adjustment essentially complete, but with incomplete adjustment to the vertical diffusion so that the depth distribution of total nitrogen is only slightly changed from the initial conditions.

[36] Figure 5 shows the vertical distribution of constituents for nine one-dimensional integrations. In the experiments shown in the top row we compare the results of integrating the three models without self-shading or vertical diffusion so that we can relate these profiles to the zero-dimensional results from sections 3 and 4. In the second row we use the results from one model, the NNPZD, to show the effects of adding first vertical diffusion, next self-shading and finally both. The last row shows the effect of changing the value of three of the parameters: R_m from 0.52 d^{-1} to 1.5 d^{-1}, Ψ from 1.46 (mmol N m^{-3})$^{-1}$ to 0, and Ω from 0.25 d^{-1} to 0.041 d^{-1}. The NNPZD model is used to illustrate these changes.

[37] Figure 5a shows the biological profiles for the NNPZD for the basic-case parameter values after 10 years of integration. Figures 5b and 5c show the results of integrating the NPZD and NPZ equations for the same time period. There is no vertical diffusion or phytoplankton self-shading in these computations. All of the features described above for the fixed-point solutions are seen in these numerical solutions. The variable $T_0(z)$ initial conditions lead to the appropriate solution for each depth z and total nitrogen $T_0(z)$. The phytoplankton reaches the $P = P^*$ solution in a surface layer for each model. The increase in T_0 with depth results in an increase in zooplankton below the surface. As the light is attenuated with depth, the phytoplankton growth slows and the amount of zooplankton that can be maintained decreases so that a zooplankton maximum is reached. Below the maximum, the zooplankton concentration decreases although the total nitrogen T continues to increase with depth. The most obvious difference among the models is the region of instability shown in the NNPZD profile. The stability of the solution at each depth predicted by the analysis of the zero-dimensional fixed points can be seen by considering a line from $z = 0$ m, $T = 10$ mmol N m^{-3} to $z = 60$ m, $T = 22$ mmol N m^{-3} on each panel of Figure 2. This line is $T = T_0(z)$, the initial condition. For the NNPZD, this line intersects region IV for a depth range of approximately $z = -40$ to -48 m. This region of instability is seen as the irregular patch in the profile (Figure 5a). Time series of the constituent values in this depth range show that the solutions at these depths are periodic in time and oscillate about the fixed point. The same line on Figures 2a and 2b for the NPZ and NPZD models does not intersect region IV consistent with the profiles that have converged to the fixed-point solution at every depth.

[38] Other features of the models shown in Figure 2 can be seen as well. For NNPZD the shallower depth range of regions III and IV for the NNPZD and the greater width of region II for large values of T compared to the other models are evident in the profile of Figure 5a. In the depth range with initial condition in region II, the 1D integration has converged to the stable fixed point with $P \neq 0$ and $Z = 0$ at each depth. This results in a smooth transition between the unstable solutions above and the stable $T = DIN = NO_3$ solutions below. In contrast, region II is very narrow for NPZD and NPZ and the transition between the stable $P = P^*$ solution and the stable $T = DIN$ solution is abrupt. The NPZD and NPZ solutions differ primarily in that the part of the total that is detritus in the NPZD solution is found in the other constituents, primarily the zooplankton, in the NPZ solution.

[39] Next, with the same $T_0(z)$ initial condition, we add vertical diffusion and phytoplankton self-shading that are absent in the zero dimensional case. *Edwards et al.* [2000] have shown that the inclusion of vertical diffusion with coefficients of the size expected in the ocean stabilizes the solutions of the NPZ model. We find that is the case for the NPZD and NNPZD models as well. Figure 5d shows

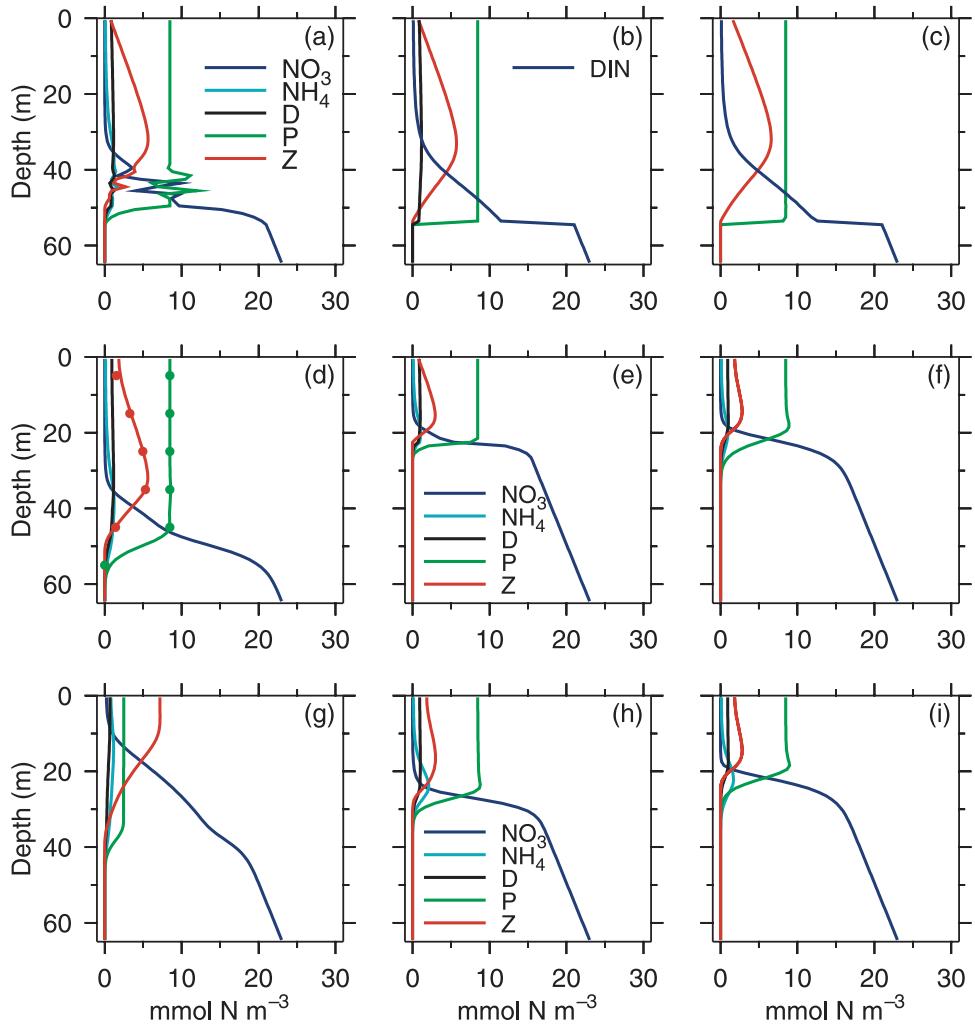

Figure 5. (top) Solutions of the ecosystem models after 10 years of integration (a) NNPZD, (b) NPZD, and (c) NPZ with $T_0(z)$ increasing linearly from 10 mmol N m^{-3} at the surface to 30 mmol N m^{-3} at $z = -100$ m. (middle) Solutions from NNPZD with $T_0(z)$ as in Figure 5a after 1 year of integration (d) with vertical diffusion, $K_B = 1 \times 10^{-6}$ m^2 s^{-1}, (e) with no vertical diffusion but with phytoplankton self-shading, $k_P = 0.0095$ m^2 (mmol N)$^{-1}$, and (f) with both weak vertical diffusion and phytoplankton self-shading. The bullets in Figure 5d are the values of the zero dimensional fixed-point solution for zooplankton and phytoplankton calculated every 10 m. (bottom) As in Figure 5f with (g) $R_m = 1.5$ d^{-1}, (h) $\Psi = 0$ (mmol N m^{-3})$^{-1}$, and (i) $\Omega = 0.041$ d^{-1}.

the NNPZD model run for 1 year with $K_B = 1 \times 10^{-6}$ m^2 s^{-1}, a small value. The bullets show the corresponding zero dimensional fixed-points values of the phytoplankton and zooplankton. We see that the fixed points are an accurate predictor of the values throughout the depth range corresponding to region IV of Figure 2c. The surface value of the zooplankton is slightly increased as nutrients are mixed into the surface and the solution adjusts to satisfy the boundary condition (equation (29)). The sharp gradients are smoothed slightly. The major effect of weak diffusion is to remove the limit-cycle solutions seen in Figure 5a.

[40] Figures 5e and 5f show the effect of adding phytoplankton self-shading first without (Figure 5e) and then with (Figure 5f) vertical diffusion. The addition of self-shading acts to decrease significantly the depths at which phytoplankton and zooplankton are found by increasing the light attenuation. For the basic-case parameter values of this study ($P^* = 8.468$), the surface layer depth is decreased by more than a factor of 2.

[41] There are no instabilities in the surface layer of Figure 5e since solutions at all light levels are stable for the total nitrogen T found in the reduced-depth surface zone. Within the layer where the phytoplankton concentration is constant with depth, adding self-shading is equivalent to increasing the value of k_w (m^{-1}) to $k_w + k_P P^*$. For the basic-case parameter values, this is an increase from 0.067 to 0.147 m^{-1}. The stability of the steady solutions can be determined by rescaling the z axis of Figure 2 to reflect this change. With no instabilities, vertical diffusion (Figure 5f) has little effect, acting only to smooth sharp gradients and increase the zooplankton very near the surface consistent with the boundary condition (equation (29)).

[42] The one-dimensional NNPZD model, including phytoplankton self-shading and weak vertical diffusion, was

also run for additional values of the parameters R_m, Ψ and Ω as listed in Table 1. The differences between the $R_m = 0.52$ d^{-1} (Figure 5f) and $R_m = 1.5$ d^{-1} (Figure 5g) are greater than that found in the zero-dimensional results. The phytoplankton self-shading is less important for $R_m = 1.5$ d^{-1} since the amount of phytoplankton in the surface layer is decreased to $P = P^* = 2.477$. This corresponds to an apparent increase in k_w from 0.067 to 0.091 m^{-1}. The region with non-zero P and Z is considerably deeper for $R_m = 1.5$ d^{-1} than for $R_m = 0.52$ d^{-1} when phytoplankton self-shading is included although the depths are comparable without self-shading. The zooplankton concentration does not increase with depth from the surface since a smaller total T is sufficient to support the zooplankton. The importance of the parameters in the zooplankton equation that change the amount of phytoplankton at steady state (γ, R_m, Λ and Γ) is enhanced when phytoplankton self-shading is included in the model.

[43] The changes to the one-dimensional solution resulting from modifying parameters that do not change the phytoplankton concentration are predictable from the zero-dimensional solutions. The change of Ψ from 1.46 to 0 $(\text{mmol N m}^{-3})^{-1}$ (Figure 5h) is consistent with the results of Appendix A with both zooplankton and phytoplankton existing at greater depths for $\Psi = 0$. The change of Ω from 0.25 to 0.041 d^{-1} (Figure 5i) results in an increase in NH_4 for the smaller Ω balanced by a decrease in NO_3 and by the smaller phytoplankton values found at depth. These differences are seen primarily in the region between about $z = -20$ m and $z = -30$ m. The surface solutions are nearly identical (compare Figures 5f and 5i).

[44] In looking at one-dimensional, depth-varying ecosystem models we find that the addition of weak vertical diffusion and self-shading by the phytoplankton can make important differences in the solutions. Any amount of vertical diffusion will, given enough time, reduce the vertical gradient in $T(z)$ to zero. With $K_B = 1 \times 10^{-6}$ m^2 s^{-1} as used in this study, integration for one year changes the $T(z)$ profile only slightly and is sufficient to stabilize the solutions so that limit cycles are not found at any depth. Phytoplankton self-shading decreases the depth of the biologically active region by increasing the light attenuation. The amount of self-shading depends on the amount of phytoplankton near the surface, thus enhancing the sensitivity of the results to the value of parameters such as R_m found in the zooplankton equation (2).

6. Mixed-Layer Model

[45] The results of the two-dimensional coupled POM-ecosystem models [*Spitz et al.*, 2003] show features that have not been included in the zero- and one-dimensional study. These features are difficult to understand in the context of a realistic model. The interactions of horizontal advection, sinking of detritus (or phytoplankton) and horizontal and vertical diffusion with the nonlinear ecosystem models result in complex distributions of the biological constituents. We develop and apply a simple biological-physical model that makes it possible to understand many of the features of the two-dimensional simulations. Recent papers that have examined the effects of physical processes on biological modeling include those by *Robinson* [1997, 1999], who considers a simple biological model and complicated flow fields. Earlier, *Klein and Steele* [1985] looked at the effect of physical processes using an NPZ model for Georges Bank in a horizontally two-dimensional flow field. They concluded that both advection and horizontal diffusion were important in determining the location of the maxima of phytoplankton and zooplankton and in determining the productivity of the system.

[46] We will look at the simplest approximation that captures the main features of the two-dimensional simulations. The realistic models are forced by upwelling-favorable wind, including time-varying wind from the summer of 1973 and the time average of that wind. This results in a mean offshore flow in a well mixed surface layer. Each of the three ecosystem models results in a nearshore maximum of phytoplankton with a patch or patches of zooplankton located offshore of the phytoplankton maximum. The values of the biological variables are largest in a surface mixed layer of about 20 m thickness. Within this layer, concentrations of zooplankton and phytoplankton are nearly uniform in the vertical. Although details change, these features are robust and are found with all three models and with both constant and time-varying wind. We attempt to model and help explain these results by considering the ecosystem equations, including idealized advection, weak horizontal diffusion and sinking of detritus or phytoplankton, averaged over the mixed layer. We assume that the concentrations of all the constituents are independent of depth within this layer and that the offshore advection velocity u is constant. The sinking rates for the detritus and phytoplankton are given in Table 1 and are the ones used by *Spitz et al.* [2003]. The sinking rate for phytoplankton in the NPZ model is chosen to be approximately as efficient as that for detritus in the other models in removing nitrogen from the surface layer for the basic-case parameters. This choice obviously depends on the remineralization rate for the detritus and, as shown below, on other parameters as well. The effect of upwelling will be included through boundary conditions at the coast.

[47] The equations for the NNPZD averaged over the mixed layer of constant depth h are

$$\frac{\partial P}{\partial t} + u\frac{\partial P}{\partial x} = \overline{G}\left(\frac{NO_3}{K_u + NO_3}\mathrm{e}^{-\Psi NH_4} + \frac{NH_4}{K_u + NH_4}\right)P + OTP + A_B\frac{\partial^2}{\partial x^2}P, \tag{30}$$

$$\frac{\partial Z}{\partial t} + u\frac{\partial Z}{\partial x} = OTZ + A_B\frac{\partial^2}{\partial x^2}Z, \tag{31}$$

$$\frac{\partial D}{\partial t} + u\frac{\partial D}{\partial x} + \frac{w_d D}{h} = OTD + A_B\frac{\partial^2}{\partial x^2}D, \tag{32}$$

$$\frac{\partial NH_4}{\partial t} + u\frac{\partial NH_4}{\partial x} = OT\,NH_4 - \overline{G}\frac{NH_4}{K_u + NH_4}P + A_B\frac{\partial^2}{\partial x^2}NH_4, \tag{33}$$

$$\frac{\partial NO_3}{\partial t} + u\frac{\partial NO_3}{\partial x} = OT\,NO_3 - \overline{G}\frac{NO_3}{K_u + NO_3}\cdot\,\mathrm{e}^{-\Psi NH_4}P + A_B\frac{\partial^2}{\partial x^2}NO_3, \tag{34}$$

where P, Z, D, NH_4 and NO_3 are the values in the mixed layer, $u = -|u|$ is the constant offshore velocity and A_B is the small, constant horizontal diffusion coefficient. In each equation, the term OTB represents the depth independent, biological terms that are not listed explicitly here (see section 2). The depth-averaged growth rate for phytoplankton $\overline{G}$ is given by

$$\overline{G} = \frac{1}{h}\int_{-h}^{0} \frac{V_m \alpha I_0 e^{-kz}}{\left(V_m^2 + \alpha^2 I_0^2 e^{-2kz}\right)^{1/2}} dz \tag{35}$$

$$= \frac{V_m}{kh} \ln\left(\frac{1 + (1 + C^2)^{1/2}}{e^{-kh} + (e^{-2kh} + C^2)^{1/2}}\right), \tag{36}$$

where

$$k = k_w + k_P P \tag{37}$$

$$C = \frac{V_m}{\alpha I_0}. \tag{38}$$

[48] The equations for NPZ and NPZD have similar forms except that in NPZ a sinking term w_p/hP is added to the left-hand side of equation (30). This formulation assumes that fluxes through the bottom of the mixed layer from vertical advection and diffusion are negligible, but includes a flux in equation (32) due to sinking of detritus.

[49] If the horizontal diffusion is neglected ($A_B = 0$), the equations can be solved by integration along characteristics. *Robinson* [1997, 1999] provides a general framework for this type of solution of ecosystem models with advection. A transformation of independent variables defined by

$$s = t,\ \xi = x - ut, \tag{39}$$

gives, for example,

$$\frac{\partial P}{\partial t} + u\frac{\partial P}{\partial x} = \frac{\partial P(s,\xi)}{\partial s}, \tag{40}$$

where the characteristics are given by the line ξ = constant. Use of the transformation (equation (39)) in equations (30)–(34) and consideration of the case $A_B = 0$ gives a set of governing ordinary differential equations in s that are integrated along the characteristic ξ = constant. The initial conditions for the integrations in s come from the initial conditions at $t = 0$, assumed to be zero, and from the upwelling boundary conditions at the coast $x = x_0$, assumed to be non-zero and constant in time. The latter are applied at $s = |u|^{-1}(\xi - x_0)$, $\xi \geq x_0$.

[50] Addition of the equations in each of the three models gives an equation for the total nitrogen $T(s)$ along the characteristic,

$$\frac{dT}{ds} = -\frac{w_d}{h} D, \tag{41}$$

for NNPZD and NPZD. For the NPZ equations, P and the phytoplankton sinking rate w_p are substituted for D and w_d on the right-hand side. This coordinate transformation leads to a system of equations that can be readily integrated. Complicated physics has been replaced by constant offshore advection. These equations can be used to understand some of the most important features of the realistic two-dimensional simulations of *Spitz et al.* [2003].

[51] Initially, to examine the effects of horizontal advection and of sinking, we will consider cases with no horizontal diffusion and obtain solutions by integration along characteristics as described above. The locations of the solution maxima and the factors influencing the zooplankton concentration will be considered in this context. Finally, we will look at the effect of small horizontal diffusion used in the two-dimensional simulations [*Spitz et al.*, 2003] and obtain solutions to equations (30)–(34) numerically using finite difference approximations.

[52] Figure 6 shows the phytoplankton and zooplankton concentration from the along characteristic integration of the three ecosystem models with $w_d = 8$ m d^{-1}, $w_p = 0.65$ m d^{-1} and mixed-layer thickness, $h = 20$ m. For an advection velocity we assume $u = 0.01$ m s^{-1} (-0.864 km d^{-1}) directed offshore. With $uh = \tau_w/\rho_0 f$, this velocity corresponds to an alongshore component of the wind stress such that $\tau_w/\rho_0 = 2.0 \times 10^{-5}$ m^2 s^{-2} where $f = 1.0 \times 10^{-4}$ s^{-1} is the Coriolis parameter. This value follows from the assumptions for u and h and is comparable to the constant alongshore wind stress $\tau^y/\rho_0 \approx 3.0 \times 10^{-5}$ m^2 s^{-2} used in the two-dimensional constant-wind simulations of *Spitz et al.* [2003]. The left-hand panels are the solutions for the basic-case parameters, in particular, $R_m = 0.52$ d^{-1}. The right-hand panels have $R_m = 1.5$ d^{-1} with the other parameters unchanged. As noted by *Spitz et al.* [2003], this change corresponds to a change from macrozooplankton to microzooplankton.

[53] The area above the slanting line is the region influenced by advection from the upwelling at the coast. The initial conditions (mmol N m^{-3}) in s applied at the coast, $x = x_0$, are (P, NO_3, Z) = (1.5, 30, 0.01) and (NH_4, D) = (0, 0) for NNPZD; (P, DIN, Z) = (1.5, 30, 0.01), $D = 0$ for NPZD; (P, DIN, Z) = (1.5, 30, 0.01) for NPZ. These values approximate those found in the nearshore upwelling region of the NNPZD two-dimensional basic-case simulation forced by constant wind [*Spitz et al.*, 2003].

[54] The most notable feature of the $R_m = 0.52$ d^{-1} solutions is the fact that the maximum zooplankton concentration is small and occurs well offshore of the phytoplankton maximum. There is little difference between the three models for the these parameters except that the magnitude of the zooplankton maximum is smaller for the NPZ. This is the reverse of the two-dimensional simulation result in which the NPZ has greater zooplankton concentration. A possible explanation for this result will be discussed below. The right-hand panels show that the results for the three models are quite similar for the larger R_m except that in this case the NPZ zooplankton concentration is larger than for the other models. For both values of R_m, the patterns of offshore maxima of zooplankton and phytoplankton are similar to those found in the two-dimensional realistic simulations [*Spitz et al.*, 2003].

[55] Figure 7 shows the total T, phytoplankton, zooplankton and DIN (or NO_3) concentrations for NPZ and NNPZD for $R_m = 0.52$ d^{-1} and $R_m = 1.5$ d^{-1} as a function of x for

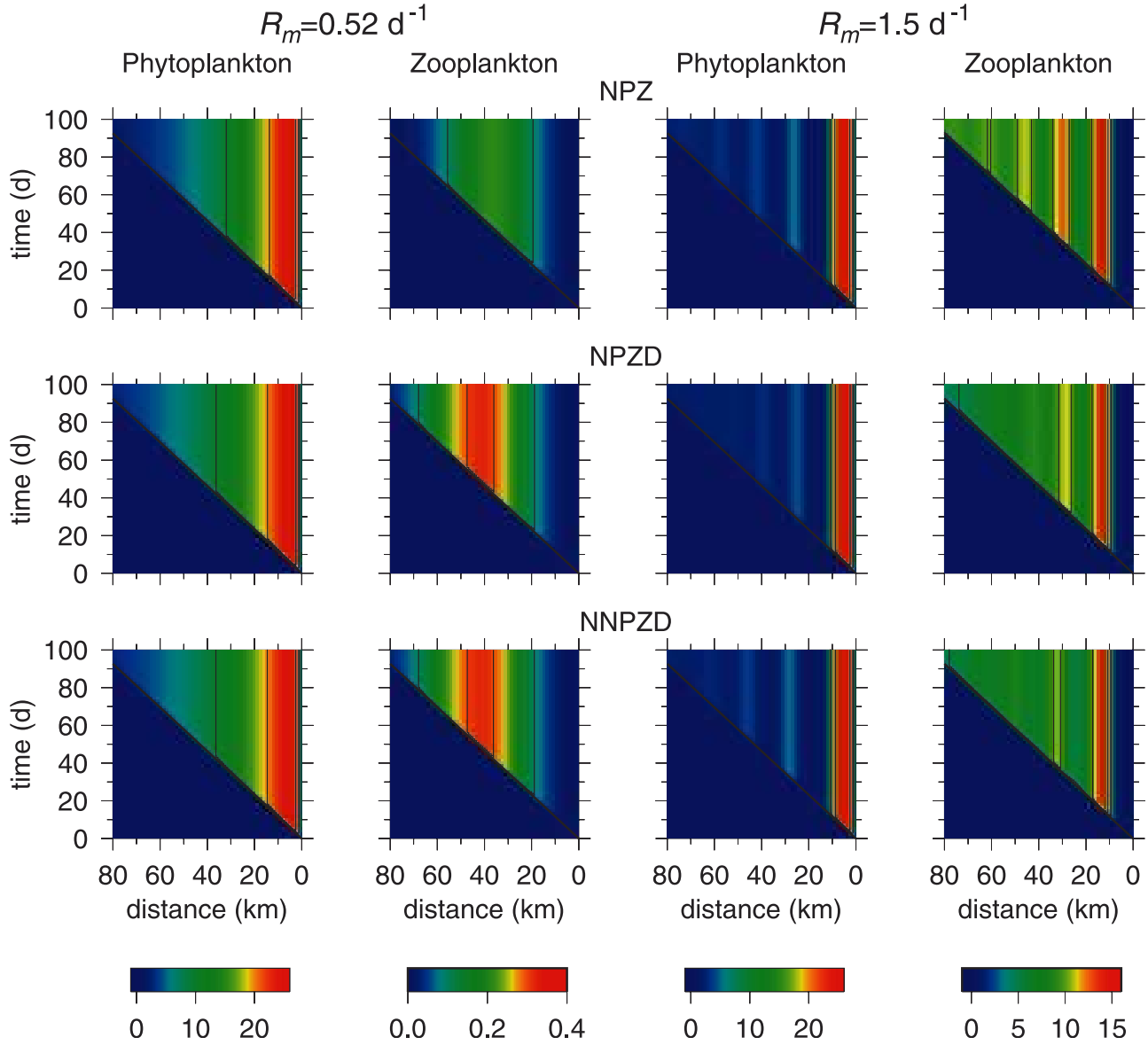

Figure 6. Solutions from integration along characteristics of the NPZ, NPZD and NNPZD mixed-layer models for mixed-layer depth 20 m and initial conditions $DIN = 30$, $P = 1.5$ and $Z = 0.01$ mmol N m^{-3} applied at the coast $x = x_0$. The scale on the horizontal axis is distance from the coast. Left panels are for the basic-case parameter values ($R_m = 0.52$ d^{-1}). The contours $P = 10$ and 20 mmol N m^{-3} and $Z = 0.1$ and 0.3 mmol N m^{-3} are shown. Right panels are for the same parameters except that $R_m = 1.5$ d^{-1}. The contours $P = 10$ and 20 mmol N m^{-3} and $Z = 5$ and 10 mmol N m^{-3} are shown. The sinking speeds are $w_d = 8$ m d^{-1} for NPZD and NNPZD and $w_p = 0.65$ m d^{-1} for NPZ.

large t (i.e., times greater than $L/|u| \approx 90$ d where L is the offshore extent of the region of interest, 80 km, and u is the advecting velocity). The results for the NPZD model, not shown, are similar to those for NNPZD. For $R_m = 0.52$ d^{-1}, the zooplankton concentration is small and has little influence on the other constituents. The detritus that sinks in the NNPZD model comes almost entirely from the phytoplankton, therefore the sinking of phytoplankton in the NPZ behaves much as the sinking of detritus in the other models. The decrease in phytoplankton with offshore distance results from the decrease of the total, that is, the sinking, rather than from biological processes. A slightly reduced sinking rate for the phytoplankton in the NPZ will result in more phytoplankton and increase the zooplankton concentration to the levels found in the other models.

[56] The case is quite different for the larger $R_m = 1.5$ d^{-1}. With the increased grazing rate, the zooplankton concentration offshore is larger than the phytoplankton concentration. The phytoplankton concentration no longer approximates the total nitrogen, but is limited by the grazing of the zooplankton. The total T decreases more slowly than in the $R_m = 0.52$ d^{-1} case for distances greater than about 20 km offshore. For the NPZ model and $R_m = 1.5$ d^{-1}, the rate of decrease of the total is proportional to the phytoplankton concentration that is smaller than for $R_m = 0.52$ d^{-1}. For NNPZD the total T with $R_m = 1.5$ d^{-1} is smaller at

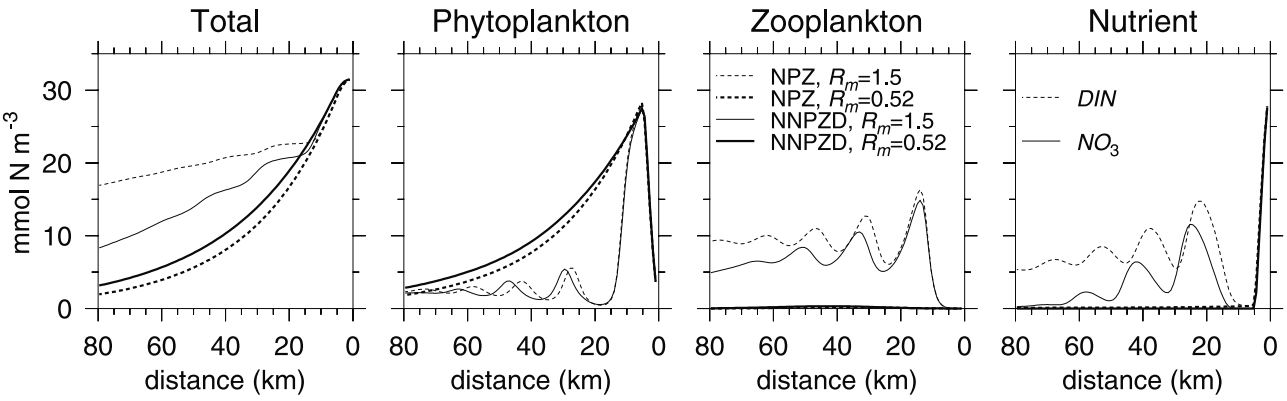

Figure 7. The variation with offshore distance for large time of total, phytoplankton, zooplankton and *DIN* or NO_3 for the NPZ (dashed lines) and NNPZD (solid) mixed-layer models with R_m = 0.52 d^{-1} (thick lines) and 1.5 d^{-1} (thin lines).

each offshore location than for the NPZ with the same parameter values, but is still larger than the total for R_m = 0.52 d^{-1}. In the NNPZD model the sinking of detritus represents a loss from both phytoplankton and zooplankton. With our choice of parameter values, the increase in the zooplankton contribution to D as R_m increases does not balance the decrease in the phytoplankton contribution so that the total nitrogen decreases slower offshore for the larger value of R_m. In the NPZ model the zooplankton egestion goes directly into the nutrient pool and remains in the mixed layer. For R_m = 0.52 d^{-1}, the zooplankton concentration is small and this difference is unimportant. For R_m = 1.5 d^{-1} a sinking rate w_p >1 m d^{-1} is required in the NPZ to remove as much nitrogen from the surface layer over the 80 km region shown in Figure 7 as is found for NNPZD.

[57] As in the R_m = 0.52 d^{-1} case, the sinking determines how far offshore the phytoplankton and zooplankton patches extend, but the location of the patches is determined by the biological processes as discussed below. A single value of w_p cannot be chosen so that the decrease in total nitrogen offshore in the surface layer is the same for the three models for the two values of R_m considered here. The value of w_p = 0.65 m d^{-1} for the NPZ results in more nitrogen removed from the surface layer for R_m = 0.52 d^{-1} and less for R_m = 1.5 d^{-1} than is found for w_d = 8 m d^{-1} in the NNPZD.

[58] The addition of sinking introduces a difference in behavior in the models that is not present in the fixed-point analysis of section 3 or the vertically one-dimensional model of section 5. This difference can result in either an increase or a decrease in the zooplankton concentration given by the NPZ relative to the other models.

[59] *Spitz et al.* [2003] consider w_d = 1 m d^{-1} as well as the basic-case value of w_d = 8 m d^{-1}. They find a moderate increase in zooplankton in the two-dimensional simulation with the smaller value of w_d. We will use w_d = 1 m d^{-1} with the other parameters at the basic-case values (Table 1) to try to understand this result (Figure 8). We use the initial conditions in s at the coast based on the NNPZD two-dimensional, basic-case simulation forced by constant wind as in Figures 6 and 7 so that these experiments are only qualitatively comparable to the w_d = 1 m d^{-1} time-varying wind experiment of *Spitz et al.* [2003].

[60] With w_d = 1 m d^{-1} and the biological parameter values unchanged (Figures 8 and 9), the maximum concentration of zooplankton is much greater than that found for w_d = 8 m d^{-1}. The zooplankton play a major role in limiting the offshore extent of the phytoplankton. We note that the maximum of the zooplankton concentration is located about 60 km offshore. Figure 8 shows that the zooplankton will not reach these levels within the time period of the two-dimensional simulation of *Spitz et al.* [2003]. This is consistent with the results in that paper of only a modest increase of zooplankton over the basic-case values.

[61] The distributions of phytoplankton and zooplankton found in the 61-day, two-dimensional simulation are qualitatively similar for the experiments with w_d = 8 m d^{-1} and 1 m d^{-1}. The mixed-layer model suggests a major difference in the time evolution with the two values of w_d. With w_d = 8 m d^{-1}, the zooplankton concentration and location for the mixed-layer averaged model is controlled by the amount of total nitrogen in the surface layer, that is the sinking speed w_d and are similar to that found in the two-dimensional simulation. This will be discussed in detail below. With w_d = 1 m d^{-1} the location and value of the zooplankton maximum found at times comparable to the integration period of the two-dimensional simulation are the result of the offshore advection speed and the length of time of the integration. Longer integration time significantly changes the mixed-layer averaged model results.

[62] To further exploit this simple mixed-layer advection model we vary the sinking rate w_d (m d^{-1}) and detritus decomposition rate Φ (d^{-1}) using the NNPZD model. These parameters interact to control the amount of nutrients present in the surface layer. The sinking physically removes detritus from the surface layer. Smaller values of w_d decrease the detritus loss from the surface layer resulting in greater nutrient concentrations. The decomposition rate determines how much of the detritus returns to the nutrient pool before it sinks. Smaller values of Φ decrease the nutrients in the surface layer. Consequently, simultaneous reduction in the values of w_d and Φ may increase the total nitrogen in the surface layer while leaving the amount of nutrients unchanged.

[63] The reduced decomposition rate for detritus Φ = 0.175 d^{-1} is chosen to give concentrations of zooplankton and phytoplankton with w_d = 1 m d^{-1} similar to those found for the basic-case mixed layer model (Figure 8). The total for

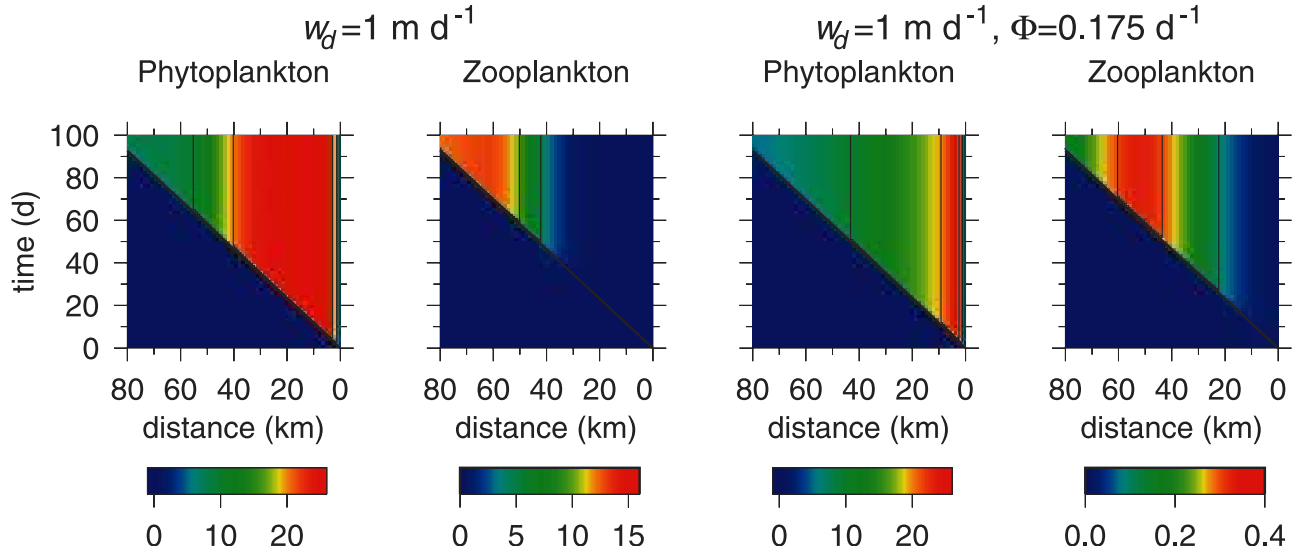

Figure 8. Solutions from integration along characteristics of the NNPZD mixed-layer model for mixed-layer depth 20 m and initial conditions $DIN = 30$, $P = 1.5$ and $Z = 0.01$ mmol N m^{-3} applied at the coast $x = x_0$. The scale on the horizontal axis is distance from the coast. Left panels are for the basic-case parameter values with sinking speed for the detritus $w_d = 1$ m d^{-1}. The contours $P = 10$ and 20 mmol N m^{-3} and $Z = 5$ and 10 mmol N m^{-3} are shown. Two right-hand panels are for the same parameter values and sinking speed except that $\Phi = 0.175$ d^{-1}. The contours $P = 10$ and 20 mmol N m^{-3} and $Z = 0.1$ and 0.3 mmol N m^{-3} are shown.

the reduced values of Φ and w_d decreases more slowly with offshore distance than does the total for the basic-case parameter values (Figure 9). This increase in the total nitrogen is contained in an increased concentration of slowly sinking, slowly decaying detritus. The concentrations of the other constituents are similar. Since measurements of detritus concentrations are problematic, differentiation of the model predictions for these two parameter-value sets would be extremely difficult in ocean applications.

[64] We now return to the basic-case parameter values and examine the results of the mixed-layer averaged model in more detail. In the two-dimensional simulations for $R_m = 0.52$ d^{-1} the NPZ model produces more zooplankton than do the NPZD and NNPZD. The mixed-layer model includes the effects of upwelling only in the coastal boundary conditions. Thus far we have used values of P, DIN and Z at the boundary that are those found in the upwelled, nearshore water of the two-dimensional NNPZD simulation forced by constant winds. Comparison of the values at the coast for the NPZ and NNPZD two-dimensional simulations forced by the same constant winds shows that the phytoplankton concentration in the upwelled water (that is at the grid point nearest the shore) is larger for the NPZ than for the NNPZD. In contrast, the zooplankton values at the coast are small and essentially equal for the two models. The increase in phytoplankton is consistent with the sinking of

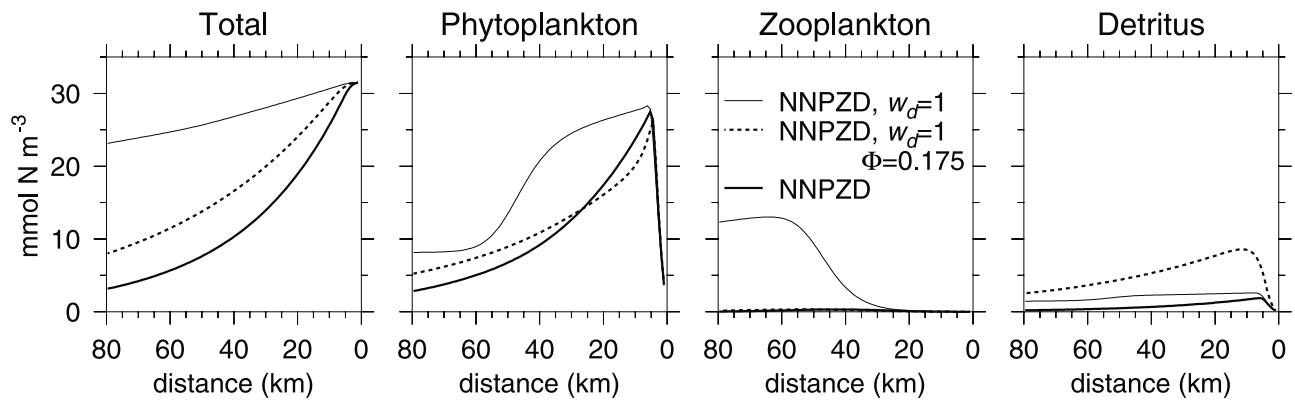

Figure 9. The variation with offshore distance for large time of total, phytoplankton, zooplankton and detritus for the NNPZD mixed-layer model with $w_d = 1$ m d^{-1}. The results of the integration with the basic-case parameter values (thin lines) and with $\Phi = 0.175$ d^{-1} (dashed lines) are shown. The NNPZD integration with the basic-case parameter values and $w_d = 8$ m d^{-1} is included for comparison (thick lines).

phytoplankton into the water being advected onshore and into the surface layer from below.

[65] We repeat the integration of the mixed-layer model NPZ with three additional sets of initial conditions in s at the coast for (P, DIN, Z). These are (4.5, 30, 0.01), (1.5, 33, 0.01) and (1.5, 30, 0.03) mmol N m^{-3}. The first set approximates the increased phytoplankton in the upwelled water seen in the two-dimensional NPZ simulation, the second has the same total nitrogen as the first with the increase in the DIN rather than in P, and the third has the original P and DIN with 3 times the Z. The total nitrogen in the boundary values is increased by 3 mmol N m^{-3} for the first two of the new boundary condition sets and by only 0.02 mmol N m^{-3} for the third. All result in an increase in zooplankton concentration from that shown in Figure 6. Increasing the phytoplankton at the boundary nearly doubles the zooplankton concentration for the NPZ model, which results in a 1.2 times increase in the zooplankton over that in the other models. Increasing the DIN results in zooplankton concentration near that of the other models. Increasing the zooplankton at the boundary increases the maximum of zooplankton by a factor of 3. The increase in zooplankton at the boundary is most efficient in increasing the final zooplankton concentration. Such an increase in zooplankton in the upwelled water, however, is not found in the two-dimensional simulations. We conclude that the increase in zooplankton found in the two-dimensional NPZ simulation is at least partly the result of the increase in phytoplankton in the upwelled water at the coast caused by the sinking of phytoplankton. Other factors not included in the mixed-layer model such as vertical advection and diffusion out of the mixed layer and changes of the depth of the mixed layer with time may also produce different effects on the different models.

[66] Recall that upwelling is included in the mixed-layer model only as imposed boundary conditions at the coast. The sensitivity of the solution of this simple model to these boundary conditions may imply that relatively small changes in the solutions of section 5 with depth can cause differences in the two-dimensional simulation. The deeper biologically active layer of the NPZ and NPZD relative to the NNPZD may result in more phytoplankton and zooplankton in the upwelled water and thus in greater productivity. Similarly, the greater concentration of phytoplankton at depth with $\Omega = 0.25$ d^{-1} or the changes with $\Psi = 0$ could be important depending on the details of the upwelling circulation. We speculate as well that the possible increase in zooplankton in the upwelled water with the inclusion of diurnal migration may be a significant feature that is not included in any of these models.

[67] Next we examine the locations of the maxima of zooplankton and phytoplankton. For simplicity we consider the NPZ model. Similar arguments hold for the other models but are less straightforward when the additional constituents are present. We find that the sharp increase in the phytoplankton concentration at about $x = 5$ km offshore is governed by

$$\frac{dP}{ds} = \overline{G}\frac{DIN}{K_u + DIN}P - \Xi P, \tag{42}$$

where we assume that the effect of sinking is small at early times so that $T = P + DIN = T(0)$ and use an average value for $\overline{G}$. Note that the zooplankton concentration remains small nearshore so that it has no effect on the phytoplankton concentration near the maximum. Integrating this equation gives an estimate of the distance along the characteristic required to reach maximum P of $s = 5.9$ d corresponding to an offshore distance of 5.1 km for an advecting velocity of $u = -0.864$ km d^{-1}. DIN decreases over this distance so that $DIN \approx T$ at the shore and $P \approx T$ at $s = 5.9$ d.

[68] The location of the zooplankton maximum for the $R_m = 0.52$ d^{-1} case is determined by the phytoplankton distribution. The extrema along the characteristic occurs for $dZ/ds = 0$, that is for the value of the phytoplankton $P = P^* = 8.468$ (equation (18)). The phytoplankton distribution offshore of the maximum of P for NPZ is essentially equal to the total nitrogen and is governed by equation (41) with P replacing T and D and with w_p replacing w_d on the right-hand side,

$$\frac{dP}{ds} = -\frac{w_p}{h}P. \tag{43}$$

Integrating equation (43) from the phytoplankton maximum at $s = 5.9$ d, we find that the phytoplankton concentration falls to the P^* value at approximately $s = 42.9$ d, corresponding to an offshore distance of 37.1 km, in good agreement with the location of the zooplankton maximum shown in Figure 6. The zooplankton concentration is estimated accurately in this case by integrating the zooplankton equation using the relationship between P and s from equation (43). This gives a maximum zooplankton concentration of 0.2 mmol N m^{-3} as does the integration along characteristics.

[69] The situation is very different for $R_m = 1.5$ d^{-1}. In this case $P^* = 2.48$ mmol N m^{-3}. Extrema in zooplankton occur at this value, but the zooplankton grazing is an important term in the phytoplankton equation and the zooplankton concentration is a significant part of the total. The estimate of the location of the phytoplankton maximum is unchanged from the $R_m = 0.52$ d^{-1} case since the zooplankton concentration is small for these relatively small values of s. The succession of offshore maxima of the biological components as s increases, T decreases and P tends to the P^* value is controlled by the coupled system of biological equations with all components including the zooplankton taking on large values. The length scale L of these oscillations is approximately 15 km. This scale can be estimated by the examination in Appendix B of the linearized solutions about the P^* fixed point of the NPZ mixed-layer averaged model (neglecting the effect of sinking). Using that analysis we estimate the length scale L (equation (B9)) of the offshore variations for $R_m = 1.5$ d^{-1} (Figures 6 and 7). We find that L varies from 14.8 km for $T_3 = 22$ mmol N m^{-3} to 13.9 km for $T_3 = 16$ mmol N m^{-3} (see Appendix B, Figure B1) in good agreement with the spacing of the maxima of the mixed-layer model.

[70] The near surface contours from the two-dimensional simulations using the NNPZD model forced by constant wind [*Spitz et al.*, 2003] show many of these features. The agreement is excellent in the $R_m = 1.5$ d^{-1} case. The extrema of the zooplankton line up near the 2.5 mmol N m^{-3} contours of the phytoplankton. Maxima with decreasing amplitude occur offshore with the first at about

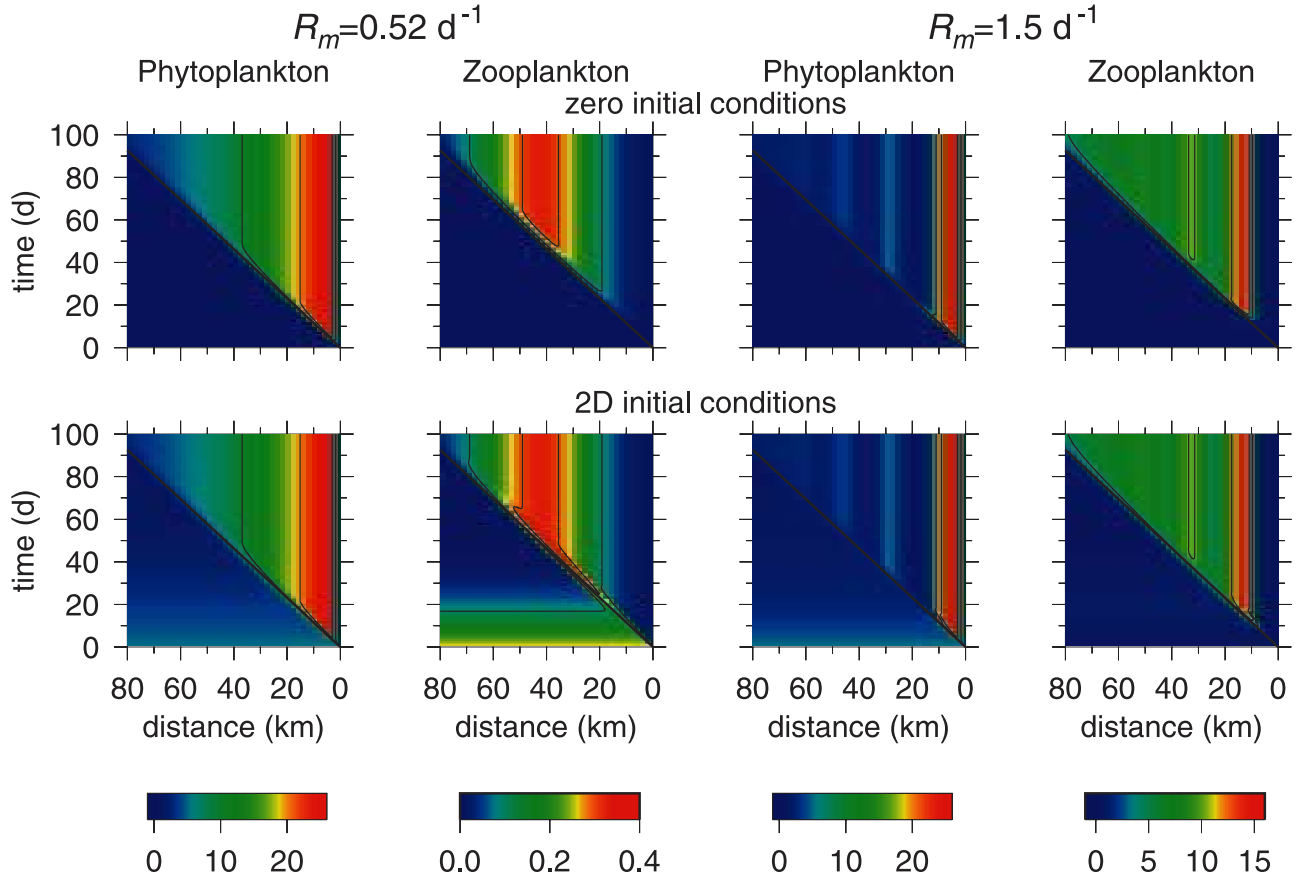

Figure 10. (top) Solutions from integration of the mixed-layer NNPZD model with horizontal diffusion with zero initial conditions at $t = 0$ and coastal boundary conditions of $DIN = 30$, $P = 1.5$ and $Z = 0.01$ mmol N m^{-3}. (bottom) Same but with initial conditions used in the two-dimensional simulation [*Spitz et al.*, 2003]. Contours and axes are as in Figure 6.

10 km and the second about 35 km offshore. The two-dimensional simulation is spun up from rest so that the patterns do not develop as rapidly as in the integration along characteristics that assumes constant offshore advection but are well established by the end of the 61-day integration.

[71] The situation for $R_m = 0.52$ d^{-1} in the two-dimensional simulations is more complicated. Figure 6 shows that the effect of the offshore advection does not reach the location of the zooplankton maximum until about day 50 of this integration. This maximum might not be expected to be fully realized in the 61-day two-dimensional integration spun up from rest. In the two-dimensional case the zooplankton maximum is found near the 15 mmol N m^{-3} contour of phytoplankton inshore of the location shown in Figure 6 at $P = P^* = 8.468$ mmol N m^{-3}. Other aspects of the two-dimensional simulation are clearly influencing the solution.

[72] Figure 10 shows the effect of the inclusion of horizontal diffusion, $A_B = 0.5$ m^2 s^{-1}, in the mixed-layer NNPZD model for both values of R_m. The top row shows the integration with an initial condition at $t = 0$ of zero for each constituent. The amplitude of the zooplankton maximum is slightly increased for $R_m = 0.52$ d^{-1} but the locations of the maxima are unchanged from the along characteristic solution shown in Figure 6. We find that the amount of the increase depends on the choice of A_B with a maximum zooplankton concentration of 0.32 mmol N m^{-3} for $A_B = 0$ m^2 s^{-1} from the along characteristic integration, 0.33 for $A_B = 0.5$ m^2 s^{-1} and 0.35 for $A_B = 2.0$ m^2 s^{-1}. There is little change from the along characteristic solution for $R_m = 1.5$ d^{-1}. The horizontal mixing across the advection front smooths the abrupt transition but the differences are minor.

[73] The second row of Figure 10 has the same initial conditions ($t = 0$) as the two-dimensional model. For $R_m = 1.5$ d^{-1}, the changes remain small with an increase in zooplankton inshore of the expected maximum at very early times. This solution is robust and determined primarily by the ecosystem model with the values of the zooplankton concentration large compared to the changes caused by the horizontal mixing. For $R_m = 0.52$ d^{-1}, an increase in the value at the zooplankton maximum at a given time over that shown in Figure 6 or the top row of Figure 10 is seen for times up to about 75 days. The location of the maximum advects offshore with time and is found inshore of the location of the $P = P^* = 8.468$ contour. This perturbation of the solution decays with time but persists throughout the time (61 days) of the two-dimensional simulation. This result is consistent qualitatively with the distribution of zooplankton found in the two-dimensional simulations with constant wind [*Spitz et al.*, 2003] where the surface zooplankton maxima were found near the location of the 15 mmol N m^{-3} phytoplankton contour.

This maximum is formed as horizontal diffusion acts to mix a small amount of the zooplankton initially present into the high phytoplankton region where it grows rapidly. The zooplankton introduced in this way adds to that advected from the upwelling region. As shown in the discussion of the choice of initial conditions for the along characteristic solution above, a small change in zooplankton in the high phytoplankton region may result in a large increase in the final zooplankton concentration.

[74] This experiment with horizontal diffusion in the mixed-layer advection model overstates the importance of this effect in the two-dimensional simulation. The initial concentration of zooplankton decreases during the spin up of the model before the upwelling circulation is established so the effect will be intermediate between that shown on the two rows of Figure 10. It is, however, clear from the location of the zooplankton maximum for $R_m = 0.52\ \mathrm{d}^{-1}$ in the two-dimensional simulation that the zooplankton distribution is not that found in the along characteristic integration of the mixed-layer advection model (no horizontal diffusion) and that the differences are consistent with horizontal mixing of the initial zooplankton distribution into the advecting high phytoplankton region.

7. Summary and Discussion

[75] The dynamics of three ecosystem models have been examined in a variety of simple situations. Each of the models is a nitrogen based system with the simplest having three components, dissolved inorganic nitrogen, phytoplankton and zooplankton; the second adds detritus and the third also includes detritus and breaks up the dissolved inorganic nitrogen into nitrate and ammonium. The models are formulated to be as much alike as possible. The intention of this work is to look at these models in increasingly complex physical situations to determine what changes in the model formulation will lead to measurable differences in realistic simulations such as those of *Spitz et al.* [2003]. We use the results of simple models, especially the mixed-layer advection model, to explain the results of the realistic simulations.

[76] The zooplankton equation is the same for the three models and includes three terms, grazing, egestion modeled as a fraction of grazing, and mortality. Each of these terms is linear in zooplankton concentration and the only other dependence is on the phytoplankton. There are other frequently used forms of this equation. In particular, a quadratic mortality term is common. This alternative formulation can be analyzed using the same techniques that we use here. The description of the results will be complicated by the fact that the phytoplankton concentration is not independent of depth whenever there is zooplankton in the system. We restrict our analysis and discussion to the equations with a linear mortality for zooplankton that are used by *Spitz et al.* [2003] and in other applications to the Oregon shelf [*Wroblewski*, 1977; *Edwards et al.*, 2000].

[77] The form of the zooplankton equation dominates the steady state solutions of the models and as seen in sections 5 and 6 is important in more complex situations as well. The only fixed points of the system with the zooplankton $Z \neq 0$ have $P = P^*$ (equation (18)). If P^* is large as in the $R_m = 0.52\ \mathrm{d}^{-1}$ case, the total amount of nitrogen in the system T must be large to support any zooplankton. Consequently, sinking, which decreases the total near the surface, may severely limit the growth of zooplankton. The value of P^* also determines the amount of phytoplankton self-shading, with large values decreasing the depth of the region with phytoplankton. As noted in many previous studies of ecosystem models, it seems certain that for ecosystem modeling to be successful the form of the zooplankton equation must be appropriate and the values of the parameters must be known accurately. We find that the importance of these parameters increases as we add realistic features such as phytoplankton self-shading and sinking of phytoplankton or detritus.

[78] The differences between models and the sensitivity to changes in the parameters not in the zooplankton equation in each model are found primarily in the deeper, low light region, below about 20 m for the depth-dependent one-dimensional case with phytoplankton self-shading. For the basic-case parameter values, the NNPZD solution phytoplankton concentration goes to zero at a shallower depth than in the other models. With no ammonium inhibition of the nitrate uptake, $\Psi = 0$, the phytoplankton in the NNPZD solution can exist deeper. Even small differences in layer depth or in the amount of zooplankton or phytoplankton at depth may be important in realistic, coupled, biological-physical models when the biomass from the deeper parts of the euphotic zone may be upwelled and moved to the surface near the coast. The size of this effect will depend on details of the upwelling circulation.

[79] The differences between the models in the zero-dimensional and one-dimensional (z dependent) cases are not large. The difference between the NPZ and the models with detritus is primarily that for the same $T(z)$ the detritus is replaced by an increase in zooplankton near the surface and by an increase in *DIN* deeper. When sinking of phytoplankton is added to the NPZ model and sinking of detritus to the other two, an additional difference is introduced.

[80] The biological model is averaged over the depth of the mixed layer and coupled with idealized physics to examine features of the two-dimensional realistic simulation. In this case, the effects of sinking are retained. Integration along characteristics agrees well with the full two-dimensional integration forced by constant wind for $R_m = 1.5\ \mathrm{d}^{-1}$ where the zooplankton growth rate is large and the biological interactions determine the concentrations and the locations of the several offshore maxima of zooplankton. This simple model reproduces the locations of the maxima of zooplankton and the offshore succession of decreasing zooplankton maxima found in the two-dimensional simulation.

[81] For $R_m = 0.52\ \mathrm{d}^{-1}$, the maximum of concentration of zooplankton in the realistic simulation occurs at a higher value of the phytoplankton than predicted by the along characteristic integration of the simple model. This implies that the location of the maxima is not solely controlled by biological processes occuring in the water advected offshore as a result of upwelling. The addition of horizontal mixing to the mixed-layer model indicates that mixing of even a small amount of zooplankton into the nearshore phytoplankton rich water can increase the magnitude of the zooplankton maximum significantly and possibly account for the difference in behavior.

[82] Other experiments with the mixed-layer model further illustrate its use as a tool to explain the results of realistic simulations. With a sinking speed for detritus of w_d = 1 m d^{-1}, *Spitz et al.* [2003] find a moderate increase in zooplankton concentration over that found with the basic-case rate with w_d = 8 m d^{-1}. The mixed-layer model indicates that the maximum of zooplankton with the reduced sinking rate would be much larger (Figure 8) and farther offshore than found in the two-dimensional simulation. This occurs, however, for times greater than the 61 day period of integration of the realistic simulation. We use the mixed-layer model to show that mean fields found with the two different sinking rates for detritus likely arise from different interactions between the physics and the biology. In one case, the rapid sinking limits the offshore extent of the zooplankton maximum. In the other with slower sinking, the speed of offshore advections determines the location of the maximum in the two-dimensional simulation. We expect that with longer integration the realistic simulation would produce larger zooplankton concentrations for the slower sinking rate.

[83] One additional case in which we reduce the decomposition rate of detritus Φ as well as the sinking speed w_d to show the coupled effects of Φ and w_d is presented. We find that all the fields except detritus predicted by the model with reduced w_d and Φ are very similar to those with the basic-case parameter values. The primary difference in the results of the reduced Φ and w_d experiment and the basic case is in the increased concentration of the detritus when it sinks and decays more slowly. This difference would be exceedingly difficult to measure.

[84] Overall, the mixed-layer model that includes both horizontal advection and sinking has proved to be a useful tool in understanding the behavior found in the two-dimensional experiments of *Spitz et al.* [2003]. Simple models of this type can be used to separate the effects of physical and biological processes. In particular, the time scales of the biological processes and of the offshore advection can be compared to understand which processes control the location of the maxima of phytoplankton and zooplankton in a particular simulation.

Appendix A: Fixed Points and Stability With Other Parameters

[85] Additional parameter values shown in Table 1 have been considered in the stability analysis. Figures A1a and A1b show the case of $\Psi = 0$ in the NNPZD with the other parameters unchanged. In particular, the parameters that are common with the other models are the same as in the basic case. For $\Psi = 0$ there is a range of depths where region I (shaded in Figure A1) ($NO_3 = T$), which is unchanged by the change in Ψ, overlaps the other three regions. There are four biologically feasible solutions at some depths in the case T = 20 mmol N m^{-3} shown in Figure A1a. In this case the solution to equation (25) at $z = -60$ m is curved so that it intersects the $P = P^*$ line inside the biologically feasible area and intersects the $Z = 0$ line for two values of P. As seen in Figure A1b the solution for T = 20 mmol N m^{-3}, $z = -60$ m is in the overlap of region I and region IV. The solution with $NO_3 = T_5$ is stable while the $P = P^*$ solution is unstable with a non-zero imaginary part indicating a periodic solution. Both solutions with $Z = 0$ are unstable. At shallower depths,

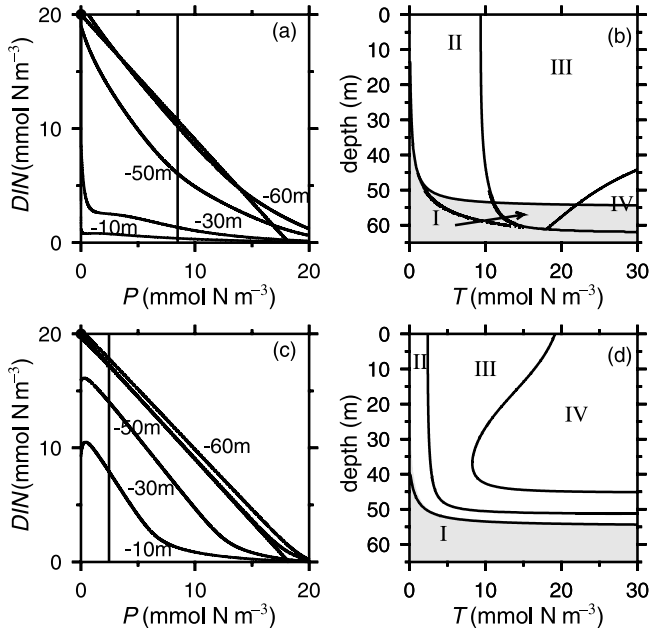

Figure A1. (a) Plots to find the approximate location of fixed points for NNPZD with $\Psi = 0$ (mmol N m^{-3})$^{-1}$ as in Figure 1. (b) Numerical calculation of regions of stability for the fixed points with $\Psi = 0$ as described in Figure 2. Region I is shaded for clarity. (c, d) As above for R_m = 1.5 d^{-1}.

for example $z = -56$ m, T = 20 mmol N m^{-3} is in the intersection of region I and region III and the $P = P^*$ solution and the $NO_3 = T_5$ solutions are both stable. Considerably more zooplankton can be supported with $\Psi = 0$ than with the basic-case value of Ψ = 1.46 (mmol N m^{-3})$^{-1}$. Steady state values of Z = 9.7, 8.8, 4.4 and 0.46 mmol N m^{-3} at $z = -10$, -30, -50 and -60 m respectively are found.

[86] Figures A1c and A1d show the effect of changing the maximum grazing rate R_m from 0.52 to 1.5 d^{-1} in the NNPZD model. This lowers the value of P^* to 2.48 mmol N m^{-3} so that phytoplankton and zooplankton can be supported at significantly smaller values of T. The size of region IV in Figure A1d is considerably larger with unstable solutions extending to the surface for moderately large values of T. The results for the other models are comparable. The amounts of zooplankton supported at steady state for T = (10, 20, 30) mmol N m^{-3} are Z = (9.0, 8.8, 5.9) and (3.1, 3.1, 2.9) at depths of -10 and -30 m, respectively. The T = 20 solutions are unstable above about 45 m. The amount of NO_3 found near the surface is greatly increased with much of the decrease in P^* going into the NO_3.

[87] The value of Ω = 0.041 d^{-1} was used by [*Wroblewski*, 1977] in his study of the Oregon upwelling region. Through most of the biologically active layer the change from Ω = 0.25 d^{-1} to Ω = 0.041 d^{-1} has little effect on the values of the constituents at the steady solution except to increase the amount of NH_4. The solutions are stable for a larger range of depths and of total nitrogen concentration T for Ω = 0.041 d^{-1}, however, with unstable solutions found only in a thin wedge at the bottom of the non-zero zooplankton region. The stable $P \neq 0$, $Z = 0$ solution is found in a nearly identical area for both choices of Ω. However, the values of P in this range are reduced for the

smaller Ω, ie $P = 1.3$ mmol N m^{-3} at $z = -52$ m for $\Omega = 0.25$ d^{-1} and 0.2 mmol N m^{-3} for $\Omega = 0.041$ d^{-1}.

Appendix B: Oscillating Solutions of NPZ

[88] For help in interpreting the results of the mixed-layer averaged model in section 6 with $R_m = 1.5$ d^{-1}, it is instructive to examine the causes of the periodic solutions found for the unstable fixed points of region IV of Figure 2 and the transient oscillations as seen in Figure 7. We will examine this in the case of the NPZ. *Busenberg et al.* [1990] calculate the fixed points and eigenvalues of the stability matrix explicitly for the NPZ model. We will look at these same equations and solutions as a damped oscillator for values of T_3 and z in regions III and IV (Figure 2a). The NPZ equations linearized about the $P = P^*$ solution in terms of the perturbation concentrations P' and DIN' are

$$\frac{dP'}{dt} = P'\left[G\frac{DIN^*}{K_u + DIN^*} - R_m Z^* \Lambda \exp\left(-\Lambda P^*\right) + R_m\left[1 - \exp\left(-\Lambda P^*\right)\right] - \Xi\right] + DIN'\left[G\frac{K_u P^*}{\left(K_u + DIN^*\right)^2} + R_m\left[1 - \exp\left(-\Lambda P^*\right)\right]\right], \tag{B1}$$

$$\frac{dDIN'}{dt} = P'\left[\gamma R_m Z^* \Lambda \exp\left(-\Lambda P^*\right). - \gamma R_m\left[1 - \exp\left(-\Lambda P^*\right)\right] + \Xi - \Gamma - G\frac{DIN^*}{K_u + DIN^*}\right] + DIN'\left[-\gamma R_m\left[1 - \exp\left(-\Lambda P^*\right)\right] - \Gamma - G\frac{K_u P^*}{\left(K_u + DIN^*\right)^2}\right]. \tag{B2}$$

[89] For the mixed-layer averaged model of section 6, the growth rate G (equation (6)) is replaced by $\overline{G}$ (equation (36)) and t with s. The change from G to $\overline{G}(P)$ involves a new dependence on the phytoplankton concentration. An additional term must be added to the linearized equations to account for this dependence. The term

$$\mathrm{NT} = P'\left(\frac{DIN^*}{K_u + DIN^*}\right)P^*\left.\frac{\partial \overline{G}}{\partial P}\right|_{(DIN^*, P^*, Z^*)} \tag{B3}$$

is added to equation (B1) and subtracted from equation (B2) to complete the linearization for the mixed-layer averaged model. Note that the sinking of phytoplankton is neglected ($w_p = 0$) so that the total $T = P^* + Z^* + DIN^*$ is not a function of s. The mixed-layer model is more stable than the zero-dimensional NPZ evaluated at the depth such that $G = \overline{G}(P^*)$ since for the mixed-layer model the growth rate for the phytoplankton decreases when the phytoplankton perturbation increases and vice versa.

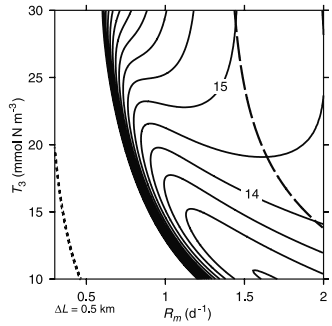

Figure B1. Contours of the length-scale L of oscillations about the P^* fixed point for the mixed-layer averaged NPZ model as a function of T_3 and R_m. The eigenvalues are real in the region where there are no solid curves. In the area below the short-dashed curve the P^* solution is not biologically feasible. In the area to the right of the long-dashed curve the P^* solution is unstable.

[90] For either the zero-dimensional NPZ or the mixed-layer averaged NPZ, we rewrite these equations as

$$\left(\frac{d}{dt} - a\right)P' = bDIN', \tag{B4}$$

$$\left(\frac{d}{dt} - d\right)DIN' = cP'. \tag{B5}$$

Multiplying equation (B4) by the operator on the left-hand side of equation (B5) we obtain a single second-order, ordinary differential equation for P',

$$\frac{d^2}{dt^2}P' - (a + d)\frac{dP'}{dt} + (ad - bc)P' = 0. \tag{B6}$$

This is the equation for a damped harmonic oscillator with undamped frequency β given by $\omega^2 = ad - bc$ and friction coefficient $r = -(a + d)$. Substituting $P' = C_0 \exp(\lambda t)$ into equation (B6) gives the equation for the eigenvalues λ of the stability matrix for NPZ,

$$\lambda^2 - (a + d)\lambda + (ad - bc) = 0. \tag{B7}$$

The solution is linearly stable if both eigenvalues have negative real part. That is, if the sum of the roots $(a + d) < 0$ and the product of the roots $(ad - bc) > 0$. The eigenvalues are complex if $(a + d)^2 - 4(ad - bc) < 0$ and the solution oscillates with frequency

$$\omega = 0.5\left|(a + d)^2 - 4(ad - bc)\right|^{1/2}. \tag{B8}$$

The oscillations decay in time if the solution is stable. For the mixed-layer model this frequency is equivalent to a length scale of offshore oscillations

$$L = 2\pi|u|/\omega, \tag{B9}$$

where $u = -0.864$ km d^{-1} is the advecting velocity in the mixed-layer model and ω is given by equation (B8).

[91] Figure B1 shows the change in the length scale L of the oscillations of the NPZ mixed-layer model with layer depth $h = 20$ m as T_3 and R_m are varied over the range of values considered in this paper. Between the dashed curves the solutions are stable and converge to the P^* solution (corresponding to region III of Figure 2a). The contours of L in this area correspond to the scale of the decaying oscillations such as shown in Figure 7. The part of the figure with no L contours corresponds to real solutions of equation (B7) and there are no oscillations. The P^* solution is unstable to the right of the long-dashed curve (region IV). Below the short-dashed line on the left the P^* solution is not biologically feasible (region II) and the analysis does not apply. The value of L is between 14 and 15 km for $R_m = 1.5$ d^{-1} and $T > 19$ mmol N m^{-3}. The solution is stable for $R_m = 1.5$ d^{-1} and $T < 24$ mmol N m^{-3}. This is consistent with the oscillations decaying offshore with the nearly uniform length scales seen in Figure 7.

[92] **Acknowledgments.** This research was supported by the National Science Foundation Coastal Ocean Processes (CoOP) Program under grants OCE-9711481 and OCE-9907854 and by the Office of Naval Research Coastal Dynamics Program under grant N00014-02-1-0100. We thank Andrew Edwards and an anonymous reviewer for their helpful comments.

References

Busenberg, S., S. K. Kumar, P. Austin, and G. Wake, The dynamics of a model of a plankton-nutrient interaction, *Bull. Math. Biol.*, *52*, 677–696, 1990.

Denman, K. L., and M. A. Peña, A coupled 1-D biological/physical model of the northeast subarctic Pacific Ocean with iron limitation, *Deep Sea Res., Part II*, *46*, 2877–2908, 1999.

Edwards, A. M., Adding detritus to a nutrient-phytoplankton-zooplankton model: A dynamical-systems approach, *J. Plankton Res.*, *23*, 389–413, 2001.

Edwards, C. A., T. M. Powell, and H. P. Batchelder, The stability of an NPZ model subject to realistic vertical mixing, *J. Mar. Res*, *58*, 37–60, 2000.

Franks, P. J. S., J. S. Wroblewski, and G. R. Flierl, Behavior of a simple plankton model with food-level acclimation by herbivores, *Mar. Biol.*, *91*, 121–129, 1986.

Klein, P., and J. H. Steele, Some physical factors affecting ecosystems, *J. Mar. Res.*, *43*, 337–350, 1985.

Nayfeh, A. H., and D. T. Mook, *Nonlinear Oscillations*, 704 pp., Wiley-Intersci., New York, 1979.

Press, W. H., S. A. Teukolsky, W. T. Vetterling, and B. P. Flannery, *Numerical Recipes in Fortran*, 963 pp., 2nd ed., Cambridge Univ. Press, New York, 1992.

Robinson, A. R., On the theory of advective effects on biological dynamics in the sea, *Proc. R. Soc. London, Ser. A*, *453*, 2295–2324, 1997.

Robinson, A. R., On the theory of advective effects on biological dynamics in the sea, II, Localization, light limitation, and nutrient saturation, *Proc. R. Soc. London, Ser. A*, *455*, 1813–1828, 1999.

Spitz, Y. H., P. A. Newberger, and J. S. Allen, Ecosystem response to upwelling off the Oregon coast: Behavior of three nitrogen-based models, *J. Geophys. Res.*, doi:10.1029/2001JC001181, in press, 2003.

Wroblewski, J. S., A model of phytoplankton plume formation during variable Oregon upwelling, *J. Mar. Res.*, *35*, 357–394, 1977.

J. S. Allen, P. A. Newberger, and Y. H. Spitz, College of Oceanic and Atmospheric Sciences, Oregon State University, 104 Ocean Administration Building, Corvallis, OR 97331, USA. (jallen@coas.oregonstate.edu; newberg@coas.oregonstate.edu; yvette@coas.oregonstate.edu)